Universitat Autònoma de Barcelona

Departament de Física

Directors del Treball de Recerca:
Verònica Ahufinger Breto i Jordi Mompart Penina

Doppler Broadened Two-Level Laser with Local Field Corrections

Daniel Viscor

<daniel.viscor@uab.es>

UAB (Barcelona), October 16, 2008

Als meus pares,
per tot el què m'han donat,
i per haver fet de mi
la persona que sóc ara.

Agraïments

En primer lloc vull agrair sincerament als meus directors del Treball de Recerca, el Jordi Mompart i la Verònica Ahufinger, tot l'interès i dedicació que han posat en aquest treball, així com la paciència que han tingut i els ànims que m'han donat quan ha calgut. També vull donar les gràcies a tots els companys del Grup d'Òptica, el Joan Bagudà, la Sònia Fernández-Vidal, l'Albert Benseny, el Ricard Menchón, l'Angel Lizana, l'Antonio Picón, l'Stefan Rist, la Isabel Santanach, el Miquel Soler, la Georgina Olivares, la Giovanna Morigi, el Gabriele De Chiara, l'Stefano Zippilli, el Ramón Corbalán, el Gaspar Orriols, el Francesc Pi, el Juan Campos i la Maria J. Yuzuel, per l'immillorable ambient de treball i pel suport, ajuda i consells que en un moment o altre m'han donat tots ells. Gràcies també a l'Alexander Pisarchik, qui em va ajudar en els inicis del treball, i que tot i la distància que hi ha hagut posteriorment ha seguit mantenint l'interès i m'ha ajudat quan ho he necessitat.

A més, vull donar les gràcies als meus pares, per tot el que han fet per mi, i també als meus germans, el Victor i la Irene, per ser una família tan fantàstica. També dono les gràcies als tiets, cosins i avis de Saragossa i Tordera per la seva preocupació, interès i estima.

Vull agrair també el costat que m'han fet i els ànims que m'han donat els meus amics, l'Ana, el Roger, la Marta, l'Albert, la Laura i l'Estel, en el procés de realització d'aquest treball, així com els bons moments que he passat amb ells durant els anys que fa que ens coneixem.

Per últim i de manera molt especial vull donar-li les gràcies a l'Anita, per haver-me fet costat en tot moment, ajudar-me, estimar-me i cuidar-me com ho ha fet fins ara.

Finalment dir que la dedicació que he posat en aquest treball ha estat possible gràcies a una beca del projecte Quantum Optical Information Technology (QOIT, Consolider Ingenio 2010) atorgada pel MEC.

Contents

1

Introduction

In the semiclassical formalism the interaction between light and matter is described by treating the light classically, i.e, by means of the Maxwell equations, and the matter quantum mechanically, i.e., using the Schrödinger equation. Two-level atomic systems interacting with an electromagnetic field have been deeply investigated in the semiclassical formalism (see for instance [1–3]) and, in spite of their simplicity, they give rise to a wide range of interesting phenomena such as Rabi oscillations, AC-Stark splitting and light-shifts [1–3]. In this research work we will investigate, using this formalism, the dynamics of a laser field generated by a two-level atomic medium including the effects of both the local field corrections [4] and the Doppler broadening [3]. On the one hand, the local field corrections, arising from near dipole dipole interactions, are typically present in dense media, where the effective field that acts on each atom is no longer the macroscopic field but the so-called local field. On the other hand, the Doppler broadening, i.e., the inhomogeneous broadening of the resonance line of the transition due to the atomic motion, has to be taken into account, in general, when dealing with optical transitions of vapors at finite temperature. These two basic concepts will be discussed in more detail in the following lines.

Local field effects arise whenever the density of the medium is high enough ($\sim 10^{17}$ at/cm^3 [5]) to make near dipole-dipole interactions important. These effects come from the fact that, at high densities, the atoms of a medium in the presence of an externally applied electromagnetic field, feel not only this macroscopic field but also the field generated by the neighboring atoms. Thus the effective field that acts on an individual atom is the so-called local field, which includes, besides the external field, the contribution of the nearby atomic dipoles. These corrections are found in the literature with the name of local field corrections and their effects have been an intense field of research during the last two

decades, both in passive systems [6–27] and in amplifying media [28–34]. The so-called generalized Maxwell-Bloch formulation [6, 7] incorporating local field effects has stimulated considerable theoretical development and predictions such as linear and non-linear spectral redshifts (Lorentz shifts) [8, 9], self-phase modulation in electromagnetically induced transparency [10], ultrafast switching effects between emission and absorption regimes [11], propagation effects in non-linear media [12], or statistical effects in superfluorescence and amplified spontaneous emission [28]. But probably the most outstanding phenomenon associated with the near dipole-dipole interactions is the intrinsic optical bistability [13]. This kind of optical bistability does not depend upon external feedback, such as cavity mirrors (for this reason this phenomenon is often called "mirrorless" optical bistability) and may be very useful in optical communications. The phenomenon of intrinsic optical bistability was first considered by Bowden and Sung [13] and studied in detail by subsequent authors [14–16, 18–20]. The necessary condition for the appearance of intrinsic optical bistability in passive systems was investigated by Friedberg *et al.* [8] who found that the near dipole-dipole parameter [21], which depends on the atomic density of the medium and the electric dipole moment of the transition, must be four times greater than the decay rate of the polarization. Thus, increasing the density of resonant atoms by itself does not necessarily provide optical bistability. Moreover, Hopf *et al.* [14] found that the density of the medium required for the appearance of intrinsic optical bistability makes the medium highly absorbent and consequently this effect can only be seen in thin media. It is important to note that there have been studies dealing with systems where intrinsic optical bistability could be more feasible. For instance, Crenshaw and Bowden [15] and Manassah [16] showed that, if the resonant atoms are embedded in a dielectric material, the effects of the local field corrections can be enhanced. This enhancement is also possible when the dense medium is composed by different species of resonant atoms, as Crenshaw, Bowden and Sullivan showed in [17]. Later, Afanas'ev *et al.* [18] showed that a dense ensemble of atoms modeled by multilevel quantum systems allows to reduce the condition [8] of appearance of intrinsic optical bistability. However, a more reachable threshold for intrinsic optical bistability is not the unique new effect that the inclusion of a multilevel system provides. For instance, in three-level systems, it was shown that the local field corrections lead to lasing without inversion and absorptionless enhancement of the refraction index [29], to density dependent switching between absorption and amplification [22], and to modification of the profile of the group

velocity and a frequency dependent transmission coefficient [23].

More recently, the effect of the local field corrections in laser instabilities has also been pointed out [30, 31], and effects of the local field corrections on spatio-temporal dynamics have been numerically studied [32, 33]. While the study by Calderón *et al.* [32] shows a cut-off on the size of the transverse structures that can appear in the dynamics of broad-area lasers, and a great complexity on the patterns, Ahufinger *et al.* [33] have found that broad-area two-level lasers are able to generate and sustain cavity solitons for high enough atomic densities. Recently, Fleischhauer *et al.* [24] have shown that, as a consequence of the local field corrections, a radiatively broadened medium with overlapping electric and magnetic resonances becomes lossless with a negative real part of the refractive index. The latter could provide an interesting avenue to construct left-handed materials with low losses. To date few experiments related with the local field corrections have been performed. However, some of them have addressed key issues arising from various theoretical developments [8, 9, 14]. Boyd and coworkers reported local field induced spectral red shifts in rubidium vapor [25], and Rand *et al.* observed intrinsic optical bistability due to local field effects in a crystal lattice highly doped with rare earth ions [26]. More recently, Eliel *et al.* studied local field effects in very high density metal vapors [27], and found excitation dependent line narrowing.

In most of the previous works the atomic medium was assumed to be homogeneously broadened. However, in our study we consider a two-level gas placed in a vapor cell, at finite temperature. In this situation the atoms are in thermal equilibrium and they move randomly in all directions, with a Maxwellian velocity distribution in the direction of the propagation of the laser field, with a mean velocity fixed by the temperature of the gas, e.g., typical values of the atomic mean velocity in a vapor cell at room temperature are 10^2-10^3 m/s. This atomic motion implies that, in general, when dealing with an optical transition, the Doppler effect has to be taken into account. As a consequence, each atom sees the laser field with a different frequency, which differs from the frequency of the field by a term proportional to the projection of the atom velocity in the propagation direction of the field. This velocity dependence in the transition frequency gives rise to a Gaussian broadening of the resonance line known as Doppler broadening. This frequency distribution is characterized by its full width at half maximum (FWHM) which is, in vapor cells at finite temperature, considerably greater than the width corresponding to the homogeneous broadening. For instance, at room

temperature and for optical transitions, typical values of the homogeneous and Doppler widths are ~ 10 MHz and ~ 1 GHz, respectively.

To date, only few articles have studied the local field effects taking into account the effect of the Doppler broadening [34, 35]. The first study was performed by Bowden *et al.* [34] who showed that in a single mode Doppler broadened laser system, the second laser threshold, which is lowered by the near dipole-dipole interaction, decreases more drastically than in the homogeneous case, making the chaotic regime more accessible. Later, Guo *et al.* [35] showed that the displacement of the resonance line due to the local field corrections [8, 9] remains significant in situations where the inhomogeneous broadening of a medium exceeds the homogeneous width.

In the present research work we analyse the role of the Doppler broadening in the dynamics of a two-level laser system, in a situation in which the density of the medium is high enough to provide intrinsic optical bistability. In this context, we study the effect of the local field corrections into the atomic population distribution, and hence, in the phenomenon known as spectral hole burning [36]. This phenomenon, that appears in Doppler broadened media, consists in the saturation of the transition of a certain group of atoms (resonant atoms) by a strong laser field. When a spectral line is Doppler broadened, a monochromatic travelling plane wave interacts only with those atoms that have a velocity projection on the travelling wave direction such that the atoms are nearly resonant with the field. The range of velocities that satisfy this condition is given by the natural broadening of the resonance line, i.e., the spontaneous emission decay rate. Hence, for this small group of atoms the absorption probability is enhanced. For a strong enough field causing saturation of the transition, the atomic population distribution is modified giving rise to a dip or hole (Bennett hole [36]), centered at the resonant velocity. This is the phenomenon known as spectral hole burning. Since the width of the hole is determined by the homogeneous width, this phenomenon is very interesting on spectroscopy [37–39] because allows to resolve fine and hyperfine structure even in the presence of a much larger Doppler widths [38, 39]. The hole burning has been studied since the earliest papers on lasers [36, 40–42]. Bennett investigated this effect [36] for the Doppler broadened amplification line of a gas laser, and Lamb [40] described the phenomenon within the context of a theoretical model for an optical maser. Hänsch *et al.* [41] observed remanent hole burning in sodium D resonance lines with a repetitively pulsed tunable dye laser, and Schawlow and Sorem [42] discussed the phenomenon in luminescent crystals, whose spectral lines

are inhomogeneously broadened at low temperatures. This phenomenon has been also studied in solid state physics, finding interesting phenomena as the luminescence hole burning [43], and persistent spectral hole burning [44, 45]. In addition, persistent spectral hole burning has been observed in quantum dots [46], and it has been used to produce electromagnetically induced transparency [47] and slow light [48]. It must be pointed out that the last results [47, 48] have also been reported in Doppler broadened atomic vapors [49, 50].

1.1 Outline

The present work is organized as follows. In Chapter 2, the theoretical background of this research work is introduced. In the first section, a detailed description of the physical system under investigation, consisting of a two-level active gas, placed in a unidirectional ring laser cavity, interacting with a single mode of an electromagnetic field, is performed. In the following sections of the chapter the optical Bloch equations, which describe the temporal dynamics of the complete system, are derived in the Semiclassical formalism. Whereas the field evolution equation is derived from the Maxwell equations under the Slowly Varying Envelope Approximation, the population and coherence evolution equations are obtained using the Schrödinger-von Neumann-Liouville formalism, under the Electric Dipole and Rotating Wave Approximations. In order to obtain a self-consistent set of equations, the polarization of the medium is assumed to act as a source term in the Maxwell equations. Finally, the local field corrections, accounting for near dipole-dipole interactions and typically present in dense media, are included in the medium equations through the Lorentz-Lorenz relation.

In Chapter 3, the steady-state solutions of the optical Bloch equations, derived in Chapter 2, including local field corrections are obtained in two different situations: the atomic medium interacting with an externally applied electromagnetic field and the medium generating a laser field itself. In the first situation we distinguish between weak and relatively strong external fields, and the number of steady-state solutions as a function of the local field corrections parameter is studied for each situation. While for the case of a weak probe field only one steady-state solution is found and the static Lorentz shift is exhibited, when a strong field is considered the system exhibit three different steady-state solutions and the dynamic Lorentz shift is observed. Next, the lasing case is considered, and again three different coexisting steady-state solutions are found for certain

parameter values of the system and the dynamic Lorentz shift is also observed. The stability of these solutions is analysed by means of a linear stability analysis, revealing an intrinsic bistable behaviour of the system above a certain threshold value of the local field corrections.

Chapter 4 deals with the inclusion of the Doppler effect in the dense two-level laser system. First, the Doppler broadening, given by the inhomogeneous broadening of a resonance line due to the atomic velocities, and the spectral hole burning, which is due to the saturation of the transition of a small group of atoms with a certain velocity, are discussed. Next, the optical Bloch equations in presence of local field corrections are generalized in order to take into account the Doppler effect. This procedure gives rise to an effective detuning which depends both on the local field corrections and on the atomic velocity, and as a consequence the velocity for which the atoms are in resonance with the field depends on the local field corrections parameter. Finally the results obtained by the integration of the generalized optical Bloch equations are presented. For local field corrections parameter values below the threshold for bistability, the main effect, including the atomic motion, is a linear displacement of the hole burning position with the parameter L. For local field corrections values above the threshold, intrinsic optical bistability is achieved and, the evolution of the two steady-state solutions for the field amplitude as a function of the Doppler width is analysed for different values of the local field corrections. The obtained behaviour is interpreted by means of the population inversion and gain profiles as a function of the atomic velocity. To finish the chapter, a discussion of the possible implementations of the studied model in realistic systems is done.

Finally, in Chapter 5, we summarize the main results and the conclusions of the research work are presented.

2

Theoretical Background

The aim of this chapter is to introduce the physical system under investigation and derive the so-called optical Bloch equations that will describe its temporal dynamics. The detailed description of the physical system setup, consisting of a pumped active gas medium placed in a unidirectional ring laser cavity, will be done in the first section (Section 2.1). Next, we will derive, in the semiclassical framework, the equations describing the dynamics of the complete system: the electromagnetic (e.m.) field (Section 2.2) and the matter (Section 2.3) time evolution equations. On the one hand, the e.m. field equation will be obtained from the Maxwell equations for a dielectric medium, under the Slowly Varying Envelope Approximation. On the other hand, the medium equations will be derived assuming the Electric Dipole and the Rotating Wave Approximations and using the von Neumann-Liouville formalism. In order to complete the description of the system, the self-consistency condition will be imposed in Section 2.4, making explicit the influence of the atomic medium in the the e.m. field dynamics. Finally, local field corrections accounting for near dipole-dipole interactions and typically present in high density media, will be introduced through the Lorentz-Lorenz relation in Section 2.5.

2.1 The Physical System

We consider the physical system sketched in Figure 2.1. It consists of an active gas medium placed inside a unidirectional ring laser cavity[1] (Figure 2.1(a)). The active gas is assumed dense enough to make dipole-dipole interactions relevant. In fact, throughout the present work, we will consider a gas density of adjustable

[1]This type of cavity gives rise to a traveling wave, thus one can avoid considering the space dependence of the field along the cavity axis.

value (N) to investigate the role of the local field effects. Moreover, the atomic medium is assumed to be formed by a collection of open two-level ($|a\rangle$ and $|b\rangle$) atoms,[2] with transition frequency ω_{ab}, interacting with a single longitudinal mode of the ring cavity, whose frequency is denoted by ω_n (Figure 2.1(b)). Spontaneous emission from the two atomic levels $|a\rangle$ and $|b\rangle$ to other atomic states at rates γ_a and γ_b, respectively, is considered, as well as a pumping process, with rate Λ, that populates the excited state, $|b\rangle$. Eventually, this pumping mechanism will be used to create population inversion.

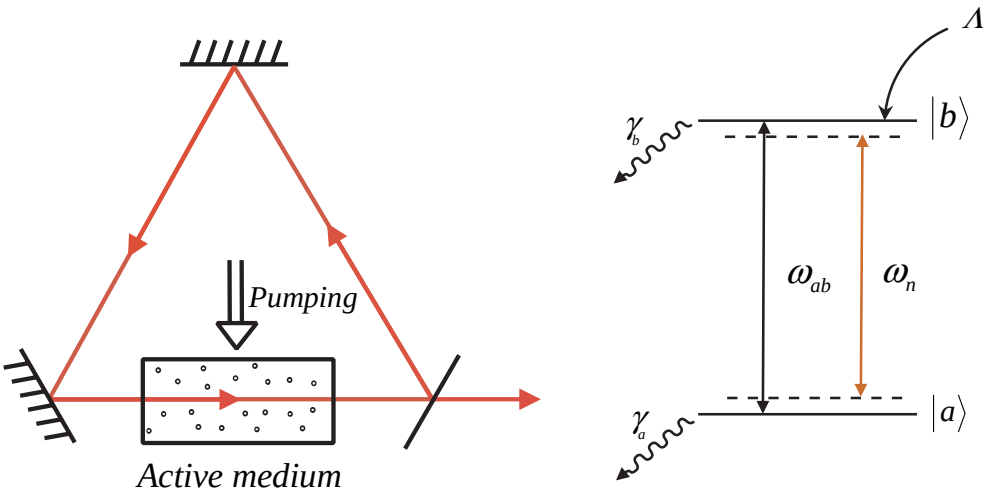

Figure 2.1: Physical system under investigation: (a) Active medium placed in a unidirectional ring cavity. (b) Open two-level ($|a\rangle$, $|b\rangle$) atom in interaction with a single e.m. mode. ω_{ab} is the transition frequency, ω_n is the e.m. mode frequency, γ_a and γ_b are the spontaneous emission decay rates and Λ accounts for the rate of the pumping mechanism that populates the upper level ($|b\rangle$) of the considered atomic transition.

2.2 Electromagnetic Field Equation

In the present section, the equation that governs the temporal dynamics of a single cavity longitudinal mode of an e.m. field propagating in a dielectric medium is derived under the Slowly Varying Envelope Approximation.

[2]The two-level approximation has been assumed, i.e., due to energy conservation and selection rules the cavity e.m. field only couples two atomic levels.

2.2.1 Maxwell Equations

The macroscopic Maxwell equations for a dielectric medium read:

$$\vec{\nabla} \times \vec{H} = \vec{J} + \frac{\partial \vec{D}}{\partial t} \tag{2.1a}$$

$$\vec{\nabla} \times \vec{E} = -\mu_0 \frac{\partial \vec{H}}{\partial t} \tag{2.1b}$$

$$\vec{\nabla} \cdot \vec{B} = 0 \tag{2.1c}$$

$$\vec{\nabla} \cdot \vec{D} = 0 \tag{2.1d}$$

where $\vec{E}$ and $\vec{B}$ are the electric field and the magnetic induction, respectively, $\vec{D} = \epsilon_0 \vec{E} + \vec{P}$ is the electric displacement with $\vec{P}$ the medium polarization, $\vec{H} = \vec{B}/\mu_0$, $\vec{J} = \sigma \vec{E}$ is the current density with σ the conductivity, and finally, ϵ_0 and μ_0 are the vacuum electric permittivity and vacuum magnetic permeability, respectively.[3] Inasmuch the medium is dielectric, like most of the optical materials, the conductivity σ should be zero. However, we assume $\sigma \neq 0$ and constant in order to modelize the losses of the laser cavity mirrors distributed along the medium.

2.2.2 Wave Equation for the Electromagnetic Field

Applying the curl to Equation (2.1b) and using Equation (2.1a) and the vectorial identity $\vec{\nabla} \times (\vec{\nabla} \times \vec{E}) = \vec{\nabla}(\vec{\nabla} \cdot \vec{E}) - \nabla^2 \vec{E}$, the wave equation for the electric field is obtained:

$$\nabla^2 \vec{E} - \mu_0 \sigma \frac{\partial \vec{E}}{\partial t} - \mu_0 \epsilon_0 \frac{\partial^2 \vec{E}}{\partial t^2} - \vec{\nabla}(\vec{\nabla} \cdot \vec{E}) = \mu_0 \frac{\partial^2 \vec{P}}{\partial t^2} \tag{2.2}$$

From Equation (2.1d) and assuming a linear response of the medium $\vec{P} = \epsilon_0 \chi \vec{E}$, where χ is the dielectric susceptibility, one obtains $\vec{\nabla} \cdot \vec{E} = 0$. Taking z as the cavity axis and assuming that the variations of the electric field in the transversal x and y directions are small compared with the wavelength, the Equation (2.2) becomes:

$$\frac{\partial^2 \vec{E}}{\partial z^2} - \mu_0 \sigma \frac{\partial \vec{E}}{\partial t} - \mu_0 \epsilon_0 \frac{\partial^2 \vec{E}}{\partial t^2} = \mu_0 \frac{\partial^2 \vec{P}}{\partial t^2} \tag{2.3}$$

Expanding the spatial part of the wave equation into normal modes of the

[3] We have assumed magnetization $\vec{M} = 0$ and magnetic permeability $\mu = \mu_0$.

form:

$$U_n(z) = \exp(iK_n z) \tag{2.4}$$

where $K_n = \omega_n^c/c$ is the wave number, ω_n^c is the angular frequency of the n-cavity mode, and $c = (\mu_0\epsilon_0)^{-1/2}$ is the speed of light in vacuum, it is easy to see that only a discrete number of longitudinal modes, satisfying the resonance condition of the cavity:

$$\omega_n^c = n\frac{2\pi c}{L} \tag{2.5}$$

can survive within the cavity, being L the length of the ring resonator and n an integer. Thus, the electric field can be written as:

$$\vec{E}(z,t) = \frac{1}{2}\sum_n \vec{E}_n(t)e^{i(K_n z - \omega_n t - \phi_n(t))} + c.c. \tag{2.6}$$

where the sum is done over all the n allowed modes, $\vec{E}_n(t)$ and $\phi_n(t)$ are the real amplitude and phase of the n mode, respectively, and $\omega_n + \dot{\phi}_n(t)$ is the oscillation frequency of the field, which is not necessarily equal to the cavity frequency ω_n^c due to the dispersion effect of the active medium.

To simplify the following analysis, we merge the real amplitude and phase of the n mode in a complex amplitude defined as $\tilde{\vec{E}}_n(t) = \vec{E}_n(t)e^{-i\phi_n(t)}$. Therefore:

$$\vec{E}(z,t) = \frac{1}{2}\sum_n \tilde{\vec{E}}_n(t)e^{i(K_n z - \omega_n t)} + c.c. \tag{2.7}$$

Accordingly, the induced polarization of the medium can be written as:

$$\vec{P}(z,t) = \frac{1}{2}\sum_n \tilde{\vec{P}}_n(t)e^{i(K_n z - \omega_n t)} + c.c. \tag{2.8}$$

where $\tilde{\vec{P}}_n(t)$ is the complex component of the polarization for the mode n, and typically is out of phase with respect to $\tilde{\vec{E}}_n(t)$. Note that the amplitudes $\tilde{\vec{E}}_n(t)$ and $\tilde{\vec{P}}_n(t)$ have been imposed to be independent of z. This assumption comes from the so-called Uniform Field Approximation [3], which considers the cavity losses distributed along the medium instead of being localized in the mirrors.

In what follows the vectorial character of the field will be neglected in expressions (2.7) and (2.8) since we assume that our medium is formed by two-level atoms, which contribute to a single polarization of the electric field [3]. Then, by inserting (2.7) and (2.8), without complex conjugates, into the wave equation (2.3),

one obtains for each mode:

$$\left[\left(\frac{\omega_n^c}{c}\right)^2 - \mu_0\epsilon_0\omega_n^2 - i\mu_0\sigma\omega_n\right]\tilde{E}_n + \left[-2i\mu_0\epsilon_0\omega_n + \mu_0\sigma\right]\dot{\tilde{E}}_n + \mu_0\epsilon_0\ddot{\tilde{E}}_n = \\ = \mu_0\omega_n^2\tilde{P}_n + 2i\mu_0\omega_n\dot{\tilde{P}}_n - \mu_0\ddot{\tilde{P}}_n \tag{2.9}$$

We assume now that the amplitudes of the fields practically do not change in a period and wavelength, i.e., we apply the Slowly Varying Envelope Approximation (SVEA) given by:

$$\left|\frac{\partial A_n}{\partial t}\right| \ll \frac{2\pi}{T}\left|A_n\right| \longrightarrow \quad \left|\frac{\partial A_n}{\partial t}\right| \ll \omega_n\left|A_n\right| \tag{2.10a}$$

$$\left|\frac{\partial^2 A_n}{\partial t^2}\right| \ll \omega_n\left|\frac{\partial A_n}{\partial t}\right| \tag{2.10b}$$

$$\left|\frac{\partial A_n}{\partial z}\right| \ll \frac{2\pi}{\lambda}\left|A_n\right| \longrightarrow \quad \left|\frac{\partial A_n}{\partial z}\right| \ll k_n\left|A_n\right| \tag{2.10c}$$

$$\left|\frac{\partial^2 A_n}{\partial z^2}\right| \ll k_n\left|\frac{\partial A_n}{\partial z}\right| \tag{2.10d}$$

where A_n is the amplitude of the considered field. Assuming that the frequency of mode n is similar to the cavity resonance frequency ($\omega_n \simeq \omega_n^c$) and using the SVEA (2.10) in Equation (2.9), the following equation for the temporal evolution of the electric field is obtained:

$$\dot{\tilde{E}}_n = -\frac{\sigma}{2\epsilon_0}\tilde{E}_n + i\frac{\omega_n}{2\epsilon_0}\tilde{P}_n \tag{2.11}$$

It is important to realize that the polarization $\tilde{P}_n$ depends implicitly on the electric field $\tilde{E}_n$ which means that equation (2.11) has to be solved in a self-consistent way. An explicit expression for the medium polarization will be derived in Section 2.4.

2.3 Medium Equations

The aim of this section is to derive the Bloch equations, from the Schrödinger-von Neumann equation, to describe the coherent evolution of a two-level medium interacting with the cavity e.m. field under the Electric Dipole and the Rotating Wave approximations. In the last part of the section, incoherent processes will be introduced phenomenologically in the equations using the Schrödinger-von Neumann-Liouville equation.

2.3.1 Coherent Dynamics

We consider the system shown in Figure 2.1(b), formed by a two-level atom interacting with a single longitudinal mode of a ring cavity. The lower and upper atomic states, with associated energies $\varepsilon_a = 0$ and $\varepsilon_b = \hbar\omega_{ab}$, respectively, are denoted by:

$$|a\rangle = \begin{pmatrix} 1 \\ 0 \end{pmatrix} \ , \ |b\rangle = \begin{pmatrix} 0 \\ 1 \end{pmatrix} \tag{2.12}$$

and therefore, the wave function of the atom can be written as:

$$|\psi(t)\rangle = c_a(t)\,|a\rangle + c_b(t)\,|b\rangle \tag{2.13}$$

where $c_a(t)$ and $c_b(t)$ are the probability amplitudes of finding the atom in the state $|a\rangle$ and $|b\rangle$, respectively.

As described in Section 2.2, the single longitudinal cavity mode of the electric field is given by the expression (2.7). The spatial dependence of the field over the size of the atom can be neglected under the Electric Dipole Approximation (EDA).[4] Therefore, assuming the atom placed at $z = 0$, the field reads:

$$\vec{E}(t) = \frac{1}{2}\vec{\tilde{E}}_n(t)e^{-i\omega_n t} + c.c. \tag{2.14}$$

where $\vec{\tilde{E}}_n(t)$ is the complex amplitude of the field and ω_n the oscillation frequency in the absence of dispersive effects of the medium.

The Hamiltonian of the system, in the Semiclassical Theory framework, consists on the sum of two terms:

$$\hat{H} = \hat{H}_0 + \hat{H}_I \tag{2.15}$$

where $\hat{H}_0$ ($\hat{H}_I$) is the free-atom (atom-field interaction) Hamiltonian. The unperturbed atomic Hamiltonian, $\hat{H}_0$, can be written in matricial form as:

$$\hat{H}_0 = \sum_{n=a}^{b} \varepsilon_n\,|n\rangle\,\langle n| = \hbar \begin{pmatrix} 0 & 0 \\ 0 & \omega_{ab} \end{pmatrix} \tag{2.16}$$

[4]The Electric Dipole Approximation allows to ignore the spatial variation of the electromagnetic field over the dimensions of the atom when the wavelength of the field is large compared with the size of the atom (Bohr radius$\sim 0.53\,$Å). This approximation is fully justified in the optical range ($\lambda \sim 1000\,$Å).

and the atom-field interaction Hamiltonian in the electric dipole interaction reads:

$$\hat{H}_I = -\hat{\vec{\mu}}\vec{E}(t) \tag{2.17}$$

where $\vec{E}(t)$ is the electric field at the position of the center of mass of the atom (2.14) and $\hat{\vec{\mu}} = q\hat{\vec{r}}$ is the atomic dipole moment operator, with q the electron charge and $\hat{\vec{r}}$ the position operator. The diagonal terms of the dipole moment operator, $\hat{\vec{\mu}}$, are in general equal to zero due to parity reasons.[5] Assuming atomic states with opposite parity, the non-diagonal elements are different from zero and therefore:

$$\hat{\vec{\mu}} = \begin{pmatrix} \vec{\mu}_{aa} & \vec{\mu}_{ab} \\ \vec{\mu}_{ba} & \vec{\mu}_{bb} \end{pmatrix} = \begin{pmatrix} 0 & \vec{\mu}_{ab} \\ \vec{\mu}_{ab} & 0 \end{pmatrix} = \vec{\mu}_{ab}\left(|a\rangle\langle b| + |b\rangle\langle a|\right) \tag{2.18}$$

where $\vec{\mu}_{ab} = \vec{\mu}_{ba}$, since $\hat{\vec{\mu}}$ is hermitic.

Then, by inserting (2.18) and (2.14) into (2.17), the interaction Hamiltonian takes the form:

$$\hat{H}_I = -\mu_{ab}\frac{\tilde{E}_n^*}{2}e^{i\omega_n t}|a\rangle\langle b| - \mu_{ab}\frac{\tilde{E}_n}{2}e^{-i\omega_n t}|b\rangle\langle a| -$$
$$-\mu_{ab}\frac{\tilde{E}_n}{2}e^{-i\omega_n t}|a\rangle\langle b| - \mu_{ab}\frac{\tilde{E}_n^*}{2}e^{i\omega_n t}|b\rangle\langle a| = \begin{pmatrix} 0 & -\tilde{\beta}^* e^{i\omega_n t} \\ -\tilde{\beta}e^{-i\omega_n t} & 0 \end{pmatrix} \tag{2.19}$$

where $\tilde{\beta} \equiv \dfrac{\mu_{ab}\tilde{E}_n}{2\hbar}$ is known as half of the Rabi frequency. Note that in (2.19), we have assumed the electric field polarized in the direction of the dipole moment. The first two terms of (2.19) correspond to the energy conserving processes where the atom is excited from $|a\rangle$ to $|b\rangle$ absorbing one photon of the field or decays from $|b\rangle$ to $|a\rangle$ emitting one photon. On the contrary, the last two terms do not conserve energy and can be eliminated under the Rotating Wave Approximation.[6]

Inserting the atomic Hamiltonian (2.16) and the atom-field interaction Hamil-

[5] In general, the wave function $u_i(\vec{r})$, corresponding to state $|i\rangle$ $(i = a, b)$ in the Schrödinger notation $\left(\psi(\vec{r},t) = c_a u_a(\vec{r}) + c_b e^{-i\omega_{ab}t}u_b(\vec{r})\right)$, has well defined parity, so inevitably $|\vec{u}_i|^2$ is a symmetric function in $\vec{r}$. Then, $\vec{\mu}_{ii} = q\int \vec{r}|\vec{u}_i|^2\, dr^3 = 0$ since $\vec{r}|\vec{u}_i|^2$ is antisymmetric.

[6] In the interaction picture, these non conserving energy terms correspond to rapidly oscillating terms (with $e^{\pm i(\omega_n+\omega_{ab})t}$) and the Rotating Wave Approximation consists in the replacement of those terms by their zero average values.

tonian (2.19) in (2.15), the Hamiltonian of the system reads:

$$\hat{H} = \hat{H}_0 + \hat{H}_I = \hbar \begin{pmatrix} 0 & -\tilde{\beta}^* e^{i\omega_n t} \\ -\tilde{\beta} e^{-i\omega_n t} & \omega_{ab} \end{pmatrix} \tag{2.20}$$

The time evolution of the state vector of the system (2.13) is governed by the Schrödinger equation:

$$\frac{d}{dt} |\psi(t)\rangle = -\frac{i}{\hbar} \hat{H} |\psi(t)\rangle \tag{2.21}$$

with $\hat{H}$ given by (2.20). However, the system can also be described by using the density matrix operator, $\hat{\rho}$:

$$\hat{\rho} = |\psi(t)\rangle \langle\psi(t)| = \begin{pmatrix} c_a c_a^* & c_a c_b^* \\ c_b c_a^* & c_b c_b^* \end{pmatrix} \tag{2.22}$$

The diagonal elements of the density matrix (2.22), ρ_{aa} (ρ_{bb}) are real and provide the probability that the atom is in the energy eigenstate $|a\rangle$ ($|b\rangle$), i.e., the population of $|a\rangle$ ($|b\rangle$). The non-diagonal elements, ρ_{ab} and ρ_{ba}, are complex numbers and determine the coherence between levels $|a\rangle$ and $|b\rangle$, being non-zero if the system is in a coherent superposition of $|a\rangle$ and $|b\rangle$.

The time evolution equation of the density matrix, i.e., the so-called Schrödinger-von Neumann equation, is then derived from the Schrödinger equation (2.21) using (2.22):

$$\frac{d\hat{\rho}}{dt} = -\frac{i}{\hbar} \left[\hat{H}, \hat{\rho}\right] \tag{2.23}$$

To obtain the density matrix time evolution equations, it would be useful to suppress the explicit temporal dependence in the Hamiltonian (2.20) by performing the following unitary transformation:

$$\hat{U}(t) = e^{i\hat{H}_2 t/\hbar} = \begin{pmatrix} 1 & 0 \\ 0 & e^{i\omega_n t} \end{pmatrix} \tag{2.24}$$

with $\hat{H}_2 = \hbar\omega_n |b\rangle \langle b|$. The transformed Hamiltonian reads:

$$\hat{\overline{H}} = \hat{U}(t)\hat{H}\hat{U}^{-1}(t) = \hbar \begin{pmatrix} 0 & -\tilde{\beta}^* \\ -\tilde{\beta} & \omega_{ab} \end{pmatrix} \tag{2.25}$$

Accordingly, the time evolution of the transformed density matrix is given by:

$$\frac{d\hat{\overline{\rho}}}{dt} = \frac{d}{dt}\left(\hat{U}(t)\hat{\rho}\hat{U}^{-1}(t)\right) = \left(\frac{d\hat{U}}{dt}\right)\hat{\rho}\hat{U}^{-1} + \hat{U}\left(\frac{d\hat{\rho}}{dt}\right)\hat{U}^{-1} + \hat{U}\hat{\rho}\left(\frac{d\hat{U}^{-1}}{dt}\right) \quad (2.26)$$

Inserting then (2.23) in (2.26), and using the definition of $\hat{U}(t)$ (2.24), the Schrödinger-von Neumann equation can be rewritten as:

$$\begin{aligned}\frac{d\hat{\overline{\rho}}}{dt} &= \left(\frac{i\hat{H}_2}{\hbar}\right)\hat{\overline{\rho}} - \left(\frac{i}{\hbar}\right)\hat{U}\left[\hat{H},\hat{\rho}\right]\hat{U}^{-1} + \hat{\overline{\rho}}\left(-\frac{i\hat{H}_2}{\hbar}\right) = \\ &= -\frac{i}{\hbar}\left[\hat{\overline{H}} - \hat{H}_2, \hat{\overline{\rho}}\right] = -\frac{i}{\hbar}\left[\hat{H}_3, \hat{\overline{\rho}}\right] \end{aligned} \quad (2.27)$$

with:

$$\hat{H}_3 = \hbar\begin{pmatrix} 0 & -\tilde{\beta}^* \\ -\tilde{\beta} & \omega_{ab} - \omega_n \end{pmatrix} = \hbar\begin{pmatrix} 0 & -\tilde{\beta}^* \\ -\tilde{\beta} & \Delta_c \end{pmatrix} \quad (2.28)$$

where $\omega_n \simeq \omega_n^c$ has been assumed, and the cavity detuning has been defined as $\Delta_c = \omega_{ab} - \omega_n^c$.

It is easy to see that the commutator in (2.27) takes the form:

$$\left[\hat{H}_3, \hat{\overline{\rho}}\right] = \hbar\begin{pmatrix} -\tilde{\beta}^*\overline{\rho}_{ba} + \tilde{\beta}\overline{\rho}_{ab} & -\tilde{\beta}^*\left(\overline{\rho}_{bb} - \overline{\rho}_{aa}\right) - \Delta_c\overline{\rho}_{ab} \\ \tilde{\beta}\left(\overline{\rho}_{bb} - \overline{\rho}_{aa}\right) + \Delta_c\overline{\rho}_{ba} & -\tilde{\beta}\overline{\rho}_{ab} + \tilde{\beta}^*\overline{\rho}_{ba} \end{pmatrix} \quad (2.29)$$

Thus, introducing (2.29) into (2.27), one obtains the time evolution equations for the populations of $|a\rangle$ and $|b\rangle$ and the coherence between these two states:

$$\dot{\overline{\rho}}_{aa} = i\left(\tilde{\beta}^*\overline{\rho}_{ba} - \tilde{\beta}\overline{\rho}_{ab}\right) = -\dot{\overline{\rho}}_{bb} \quad (2.30a)$$

$$\dot{\overline{\rho}}_{ab} = i\tilde{\beta}\left(\overline{\rho}_{bb} - \overline{\rho}_{aa}\right) + i\Delta_c\overline{\rho}_{ab} = \left(\dot{\overline{\rho}}_{ba}\right)^* \quad (2.30b)$$

2.3.2 Incoherent Processes

In the previous subsection the medium equations have been derived taking into account only the coherent contribution of the atom-field interaction. However, there are incoherent processes affecting the dynamics of the system, e.g., spontaneous emission and incoherent pumping, that should be taken also into account. In the semiclassical formalism, these processes can be included phenomenologically in the Schrödinger-von Neumann equation (2.27) through the Liouville operator $\Gamma\hat{\overline{\rho}}$

yielding:

$$\frac{d\hat{\overline{\rho}}}{dt} = -\frac{i}{\hbar}\left[\hat{H}_3, \hat{\overline{\rho}}\right] + \Gamma\hat{\overline{\rho}} \tag{2.31}$$

For the two-level atom under consideration (Figure 2.1(b)) the matrix elements of the Liouville operator $\Gamma\hat{\overline{\rho}}$ are:

$$\langle a|\,\Gamma\hat{\overline{\rho}}\,|a\rangle = -\gamma_a\overline{\rho}_{aa} \tag{2.32a}$$
$$\langle b|\,\Gamma\hat{\overline{\rho}}\,|b\rangle = -\gamma_b\overline{\rho}_{bb} \tag{2.32b}$$
$$\langle a|\,\Gamma\hat{\overline{\rho}}\,|b\rangle = -\Gamma_{ab}\overline{\rho}_{ab} \tag{2.32c}$$
$$\langle b|\,\Gamma\hat{\overline{\rho}}\,|a\rangle = -\Gamma_{ba}\overline{\rho}_{ba} = -\Gamma_{ab}\overline{\rho}_{ba} \tag{2.32d}$$

where the rates γ_a and γ_b account for the population decay by spontaneous emission from $|a\rangle$ and $|b\rangle$, respectively, to external levels and Γ_{ab} is the decay rate of the coherence between levels $|a\rangle$ and $|b\rangle$. Note that $\Gamma_{ba} = \Gamma_{ab}$ since $\overline{\rho}_{ab} = \overline{\rho}^*_{ba}$. For simplicity we will assume that $\gamma_a = \gamma_b = \gamma$. To find a relationship between Γ_{ab} and γ let us recall that:

$$\overline{\rho}_{ii} = c_i c_i^* \tag{2.33a}$$
$$\overline{\rho}_{ij} = c_i c_j^* \tag{2.33b}$$

where $i, j = \{a, b\}$. Let us take the time derivative of (2.33a) and us the matrix element $(\Gamma\rho)_{ii}$:

$$\dot{c}_i c_i^* + c_i \dot{c}_i^* = -\gamma c_i c_i^* \tag{2.34}$$

Then, imposing that the coefficient c_i evolves like:

$$\dot{c}_i = -A_i c_i \tag{2.35}$$

with $A_i = ct$, and inserting (2.35) into (2.34), we find that $A_a = A_b = \frac{\gamma}{2}$.

Performing the time derivative of the expression (2.33b) and using (2.35) with the previous expressions of A_i, we obtain $\Gamma_{ab} = \gamma$. Throughout the derivation of this coherence decay term, only the spontaneous emission has been considered, i.e., we have assumed the radiative limit. However, there exist other mechanisms that, despite preserving the populations, also produce a decrease in the coherence. The elastic collisions are one of these effects that should be considered, particularly

in dense media. During an elastic collision, the continuous coherent interaction between the atom and the e.m. wave is interrupted, causing phase jumps in the wave function of the atom and, therefore, affecting the coherence between the atomic levels. This collisional effect will be taken into account by introducing an additional rate γ_{col} in Γ_{ab}. Thus, we define a generic coherence decay rate $\gamma_\perp$ that include the coherence decay due to both spontaneous emission and elastic collisions:

$$\gamma_\perp = \Gamma_{ab} + \gamma_{col} \tag{2.36}$$

The complete set of equations for the temporal evolution of the atomic populations and coherences for the two-level system read:

$$\dot{\overline{\rho}}_{aa} = i(\tilde{\beta}^* \overline{\rho}_{ba} - \tilde{\beta}\overline{\rho}_{ab}) - \gamma \overline{\rho}_{aa} \tag{2.37a}$$

$$\dot{\overline{\rho}}_{bb} = -i(\tilde{\beta}^* \overline{\rho}_{ba} - \tilde{\beta}\overline{\rho}_{ab}) - \gamma \overline{\rho}_{bb} + \Lambda \tag{2.37b}$$

$$\dot{\overline{\rho}}_{ab} = i\tilde{\beta}^* (\overline{\rho}_{bb} - \overline{\rho}_{aa}) + i\Delta_c \overline{\rho}_{ab} - \gamma_\perp \overline{\rho}_{ab} = (\dot{\overline{\rho}}_{ba})^* \tag{2.37c}$$

where the pumping rate Λ, which populates the upper level $|b\rangle$, has been included in (2.37b) phenomenologically.

2.4 Polarization of the Medium

We have shown in Section 2.2, that the field evolution equation (2.11) depends explicitly on the polarization of the medium. In order to provide a complete description of the system, we derive in this section an expression for this polarization. The cavity electric field induces microscopic electric dipole moments in the active medium whose sum yields the macroscopic polarization of the medium, which acts as a source term in the Maxwell equations. The condition of self-consistency then requires that the original field equals the reaction field.

Let us begin defining the macroscopic polarization per unit volume as the contribution of all the atomic electric dipole moments, $\hat{\mu}_l$, within that volume:

$$P = N \sum_l \langle \hat{\mu} \rangle_l = N \sum_l Tr\left(\hat{\rho}_l \hat{\mu}\right) \tag{2.38}$$

where N is the density of active atoms and we have used the definition of the expected value of an operator in the density matrix formalism. Here $\hat{\rho}_l$ is the

microscopic density operator associated to each atom.

We also define the macroscopic density operator as the statistical summation of the microscopic density operators:

$$\hat{\rho} = \sum_{l} \hat{\rho}_l \tag{2.39}$$

Then, combining (2.38) and (2.39) the macroscopic polarization takes the form:

$$P = NTr\left(\hat{\rho}\hat{\mu}\right) = N\left(\rho_{ab}\mu_{ba} + \rho_{ba}\mu_{ab}\right) \tag{2.40}$$

This macroscopic polarization of the medium arises from the contribution of all the dipole moments induced by the field. According to the self-consistency condition it must equal the polarization field acting as a source term in the wave equation for the electric field derived from the Maxwell equations (2.2). Considering only one mode and using the Electric Dipole Approximation, the polarization field (2.8) can be rewritten as:

$$P(t) = \frac{1}{2}\tilde{P}_n e^{-i\omega_n t} + c.c. \tag{2.41}$$

In order to compare both polarizations, (2.40) and (2.41), we introduce the temporal dependence in the first one by performing the following unitary transformation of the density matrix:

$$\hat{\rho} = U^{-1}(t)\hat{\overline{\rho}}U(t) = \begin{pmatrix} \overline{\rho}_{aa} & \overline{\rho}_{ab}e^{i\omega_n t} \\ \overline{\rho}_{ba}e^{-i\omega_n t} & \overline{\rho}_{bb} \end{pmatrix} \tag{2.42}$$

where the unitary operator $U(t)$ has been defined in (2.24). Then, using this transformed density operator in (2.40), the macroscopic polarization becomes:

$$P(t) = N\left(\mu_{ba}\overline{\rho}_{ba}e^{-i\omega_n t} + \mu_{ab}\overline{\rho}_{ab}e^{i\omega_n t}\right) \tag{2.43}$$

By comparing expressions (2.41) and (2.43) we obtain:

$$\tilde{P}_n = 2N\mu_{ab}\overline{\rho}_{ba} \tag{2.44}$$

Finally, inserting this expression for the amplitude of the polarization into the

field evolution equation (2.11) we obtain:

$$\dot{\tilde{E}}_n = -\frac{\sigma}{2\epsilon_0}\tilde{E}_n + i\frac{\omega_n}{2\epsilon_0}2N\mu_{ab}\overline{\rho}_{ba} \tag{2.45}$$

In order to rewrite this expression in a compact form, let us define:

$$g = \frac{N\omega_n \left|\mu_{ab}\right|^2}{2\hbar\epsilon_0} \tag{2.46a}$$

$$\kappa_0 = \frac{\sigma}{2\epsilon_0} \tag{2.46b}$$

as the gain parameter and the cavity losses, respectively. Then, using the definition $\tilde{\beta} = \frac{\mu_{ab}\tilde{E}_n}{2\hbar}$, known as the half of the Rabi frequency, the field evolution equation (2.45) takes the form:

$$\dot{\tilde{\beta}} = -\kappa_0\tilde{\beta} + ig\overline{\rho}_{ba} \tag{2.47}$$

2.5 Local Field Corrections

In rarefied media the average distance between atoms/molecules is so large that the macroscopic electric field and the field acting on any atom are practically equal. However, in dense media, the polarization of the neighboring atoms gives rise to an effective field, named local field or Lorentz field. The relationship between the local field and the external field is given by the Lorentz-Lorenz relation [4]:

$$\vec{E}' = \vec{E} + \left(\frac{1}{3\epsilon_0} + s\right)\vec{P} \tag{2.48}$$

where s is the structure factor that accounts for the correlations of atomic positions that occur in crystals, and is equal to zero in highly symmetric lattices. In addition, it is also generally assumed to be equal to zero for amorphous media, e.g., atomic gases. Therefore, in what follows:

$$\vec{E}' = \vec{E} + \frac{\vec{P}}{3\epsilon_0} \tag{2.49}$$

Let us consider an e.m. field $\vec{E}$ and the induced polarization $\vec{P}$ as:

$$\vec{E} = \frac{1}{2}\vec{\tilde{E}}_n e^{-i\omega_n t} + c.c. \tag{2.50a}$$

$$\vec{P} = \frac{1}{2}\vec{\tilde{P}}_n e^{-i\omega_n t} + c.c. \tag{2.50b}$$

Assuming $\vec{E}$ and $\vec{P}$ parallel, and using (2.44) one obtains:

$$E' = \left(\frac{1}{2}\tilde{E}_n + \frac{N\overline{\rho}_{ba}\mu_{ab}}{3\epsilon_0}\right) e^{-i\omega_n t} + c.c. \tag{2.51}$$

which introduced in the atom-field interaction Hamiltonian (2.17) and following the same procedure as in Section 2.3 leads to the following Hamiltonian of the system:

$$\hat{H}_3 = \hbar \begin{pmatrix} 0 & -\left(\tilde{\beta}^* + LFC\rho_{ab}\right) \\ -\left(\tilde{\beta} + LFC\rho_{ba}\right) & \Delta_c \end{pmatrix} \tag{2.52}$$

where we have defined

$$LFC = \frac{|\mu_{ab}|^2 N}{3\hbar\epsilon_0} \tag{2.53}$$

Finally, inserting (2.52) into the Schrödinger-von Neumann-Liouville equation (2.31) the density matrix equations including local field corrections are obtained:

$$\dot{\overline{\rho}}_{aa} = i(\tilde{\beta}^*\overline{\rho}_{ba} - \tilde{\beta}\overline{\rho}_{ab}) - \gamma\overline{\rho}_{aa} \tag{2.54a}$$

$$\dot{\overline{\rho}}_{bb} = -i(\tilde{\beta}^*\overline{\rho}_{ba} + \tilde{\beta}\overline{\rho}_{ab}) - \gamma\overline{\rho}_{bb} + \Lambda \tag{2.54b}$$

$$\dot{\overline{\rho}}_{ab} = i\tilde{\beta}^*(\overline{\rho}_{bb} - \overline{\rho}_{aa}) + iLFC\overline{\rho}_{ab}(\overline{\rho}_{bb} - \overline{\rho}_{aa}) + i\Delta_c\overline{\rho}_{ab} - \gamma_\perp\overline{\rho}_{ab} = (\dot{\overline{\rho}}_{ba})^* \tag{2.54c}$$

Notice that the local field corrections only appear explicitly in the equation of the atomic coherences, as a non-linear detuning depending on the population difference.

2.5.1 Normalization of the Optical Bloch Equations

The optical Bloch equations, that describe the dynamics of the complete system, contain the density matrix (2.54) and the field (2.47) equations:

$$\dot{\overline{d}} = -4\,\mathrm{Im}(\tilde{\beta}\overline{\rho}_{ab}) - \gamma\overline{d} + \Lambda \tag{2.55a}$$

$$\dot{\overline{\rho}}_{ab} = i\tilde{\beta}^{*}\overline{d} + iLFC\overline{\rho}_{ab}\overline{d} + i\Delta_c\overline{\rho}_{ab} - \gamma_{\perp}\overline{\rho}_{ab} = \left(\dot{\overline{\rho}}_{ba}\right)^{*} \tag{2.55b}$$

$$\dot{\tilde{\beta}} = -\kappa_0\tilde{\beta} + ig(\overline{\rho}_{ab})^{*} \tag{2.55c}$$

where we have defined the new variable $\overline{d} = \overline{\rho}_{bb} - \overline{\rho}_{aa}$ as the population inversion.

Equations (2.55) can be written in a normalized form by defining:

$$\rho_{10} = \frac{g_0\overline{\rho}_{ab}}{\gamma_{\perp}^2} \tag{2.56a}$$

$$d = \frac{g_0\overline{d}}{\gamma_{\perp}^2} \tag{2.56b}$$

$$\tilde{\alpha} = \frac{\tilde{\beta}}{\gamma_{\perp}} \tag{2.56c}$$

$$\tau = t\gamma_{\perp} \Longrightarrow \frac{d}{d\tau} = \frac{1}{\gamma_{\perp}}\frac{d}{dt} \tag{2.56d}$$

$$\tilde{\sigma} = \frac{\kappa_0}{\gamma_{\perp}} \tag{2.56e}$$

where

$$g_0 = \frac{N_0\omega_n\left|\mu_{ab}\right|^2}{2\hbar\epsilon_0} \tag{2.57}$$

is the gain parameter corresponding to a reference value for the density of the medium, N_0.

The normalized equations read:

$$\dot{d} = b(r - d) - 4\,\mathrm{Im}(\tilde{\alpha}\rho_{10}) \tag{2.58a}$$

$$\dot{\rho}_{10} = i\tilde{\alpha}^{*}d - [1 - i(\tilde{\Delta}_c + Ld)]\rho_{10} \tag{2.58b}$$

$$\dot{\tilde{\alpha}} = -\tilde{\sigma}\tilde{\alpha} + ip(\rho_{10})^{*} \tag{2.58c}$$

where $L = \gamma_{\perp}p/3\omega_n$ corresponds to the local field corrections parameter, being $p = N/N_0$ the ratio between the density of the active medium N and the reference value N_0. Moreover, the normalized pump rate becomes $r = g_0\Lambda/\gamma_{\perp}^2\gamma$, the normalized cavity detuning $\tilde{\Delta}_c = \Delta_c/\gamma_{\perp}$, and the decay rate of the population inversion $b = \gamma/\gamma_{\perp}$. The normalization chosen in (2.58) is different from the usual way to normalize the two-level laser equations [30, 31], in order to keep the explicit

dependence of the local field corrections parameter with the atomic density. This dependence is made explicit in our case through the parameter p.

Notice that the local field corrections term included in (2.58b) can be interpreted as a non-linear detuning ($\Delta^s = Ld$). As we will discuss in the next chapter, this term yields the Lorentz shift and, depending on the parameters, intrinsic optical bistability.

3

Steady-State Solutions and Linear Stability Analysis

In this chapter, the role of the local field corrections (LFC) in the two-level laser dynamics is analysed. First, in Section 3.1, the steady-state solutions of the optical Bloch equations, derived in Chapter 2, are found, and a discussion of the static (Subsection 3.1.1) and the dynamic (Subsection 3.1.2) Lorentz shifts is performed. In the latter case, the non-linear shift of the frequency of the atomic transition gives rise, above a threshold value for the atomic density, to three different coexisting steady-state solutions; one trivial solution corresponding to a non-lasing state, and two lasing solutions. In the last section (Section 3.2), the stability of these three steady-state solutions is studied by means of a Linear Stability Analysis. The results reveal an intrinsic bistable behaviour of the system within a certain range of the cavity detuning parameter: the non-lasing and one of the lasing solutions are both stable while the other non-trivial solution is always unstable.

3.1 Solutions of the System

It has been shown [8, 9] that, in the context of the amplification of a probe field interacting with a two-level atomic medium, the inclusion of the local field corrections (LFC) in the Bloch equations gives rise to a non-linear shift in the frequency of the atomic transition proportional to the population inversion d, i.e., the so-called Lorentz shift:

$$\Delta^s = Ld \tag{3.1}$$

where L is the LFC parameter defined after (2.58). In the case of a weak probe field, the population inversion is constant for all field detunings, and hence the

resonance line shape is shifted as a whole with a constant value. This well known effect is named static Lorentz shift. In contrast, if the applied field is intense enough, the population distribution of the levels depends strongly on the detuning, and therefore the shift varies along the resonance line shape, giving rise to the so-called dynamic Lorentz shift.

In this section the steady-state solutions of the two-level optical Bloch equations derived in Chapter 2 (2.58) are obtained and both the static and the dynamic Lorentz shifts are illustrated. In order to determine the stationary solutions of the equations (2.58) it is convenient to use the following equivalent set of equations by expressing the field as a real amplitude and phase and separating the real and complex parts of the atomic coherence:

$$\dot{d} = b\,(r - d) - 4\alpha Y_{10} \tag{3.2a}$$

$$\dot{X}_{10} = -\left(\tilde{\Delta} + Ld\right) Y_{10} - X_{10} \tag{3.2b}$$

$$\dot{Y}_{10} = \alpha d + \left(\tilde{\Delta} + Ld\right) X_{10} - Y_{10} \tag{3.2c}$$

$$\dot{\alpha} = -\tilde{\sigma}\alpha + pY_{10} \tag{3.2d}$$

$$\tilde{\Delta} = \tilde{\Delta}_c + p\frac{X_{10}}{\alpha} \tag{3.2e}$$

where d is the population inversion, X_{10} and Y_{10} are the real and imaginary parts of the coherence, respectively, α is the modulus of the amplitude of the generated field, and $\tilde{\Delta} = [\omega_{ab} - (\omega_n + \dot{\phi})]/\gamma_\perp$ is the field detuning, which differs from the cavity detuning $\tilde{\Delta}_c = [\omega_{ab} - \omega_n^c]/\gamma_\perp$ due to the dispersive effects of the medium, $\dot{\phi}$. The rest of the parameters are as in (2.58): b is the decay rate of the population inversion, r is the pump rate, L is the local field corrections parameter, p is the gain parameter, and $\tilde{\sigma}$ are the cavity losses.

Notice that (3.2) is a set of five real equations which are not independent: the phase of the field (or the field detuning, $\tilde{\Delta}$) is completely determined with the knowledge of the other variables. Therefore one can look for a set of four independent real differential equations, by inserting (3.2e) into (3.2b) and (3.2c):

$$\dot{d} = b\,(r - d) - 4\alpha Y_{10} \tag{3.3a}$$

$$\dot{X}_{10} = -\left(\tilde{\Delta}_c + p\frac{X_{10}}{\alpha} + Ld\right) Y_{10} - X_{10} \tag{3.3b}$$

$$\dot{Y}_{10} = \alpha d + \left(\tilde{\Delta}_c + p\frac{X_{10}}{\alpha} + Ld\right) X_{10} - Y_{10} \tag{3.3c}$$

$$\dot{\alpha} = -\tilde{\sigma}\alpha + pY_{10} \tag{3.3d}$$

3.1.1 Static Lorentz Shift

It is well known that, in a two-level atomic medium, the natural broadening of the energy levels, which is due to the spontaneous emission phenomenon, gives rise to a Lorentzian profile in the absorption/amplification spectrum of the medium (dotted curve in Figure 3.1). This curve is centered at the transition frequency of the two-level atom, and its full width at half maximum is the sum of the spontaneous emission rates of the upper and lower levels. In order to study the effect of the local field corrections in the absorption spectrum of a weak probe electromagnetic field of amplitude α_w and frequency ω_w, interacting with our gas of two-level atoms, we rewrite the Bloch equations (3.2a)-(3.2c) as:

$$\dot{d} = b\,(r - d) - 4\alpha_w Y_{10} \tag{3.4a}$$

$$\dot{X}_{10} = -\left(\tilde{\Delta}_w + Ld\right) Y_{10} - X_{10} \tag{3.4b}$$

$$\dot{Y}_{10} = \alpha_w d + \left(\tilde{\Delta}_w + Ld\right) X_{10} - Y_{10} \tag{3.4c}$$

where $\tilde{\Delta}_w = [\omega_{ab} - \omega_w]/\gamma_\perp$ is the probe field detuning. It is important to realise that, since the probe field comes from an external source, the amplitude and the phase can be considered now as constants, and thus α_w and $\tilde{\Delta}_w$ are parameters, rather than variables.

Setting all time derivatives of equations (3.4) equal to zero, the steady-state solution of the system can be obtained from the following equation for the imaginary part of the atomic coherence:

$$AY_{10}^3 + BY_{10}^2 + CY_{10} + D = 0 \tag{3.5}$$

where

$$A = -\frac{16L^2\alpha_w^2}{b^2} \tag{3.6a}$$

$$B = \frac{8\alpha_w L}{b}\left(Lr + \tilde{\Delta}_w\right) \tag{3.6b}$$

$$C = -\left[1 + L^2r^2 + 2\tilde{\Delta}_w Lr + \tilde{\Delta}_w^2 + \frac{4\alpha_w^2}{b}\right] \tag{3.6c}$$

$$D = \alpha_w r \tag{3.6d}$$

The discriminant of equation (3.5), denoted by δ, reads:

$$\delta = -4DB^3 + B^2C^2 - 4AC^3 + 18ABCD - 27A^2D^2 \tag{3.7}$$

It can be shown from the coefficients (3.6) that δ is negative for a wide range of parameter values, leading to only one real solution, but in the case of a probe field with an intensity similar to the coherence decay rate b, i.e., $\alpha_w^2 \sim b$, positive values of δ can be found, and then three different real solutions of (3.5) are found, as we will discuss later.

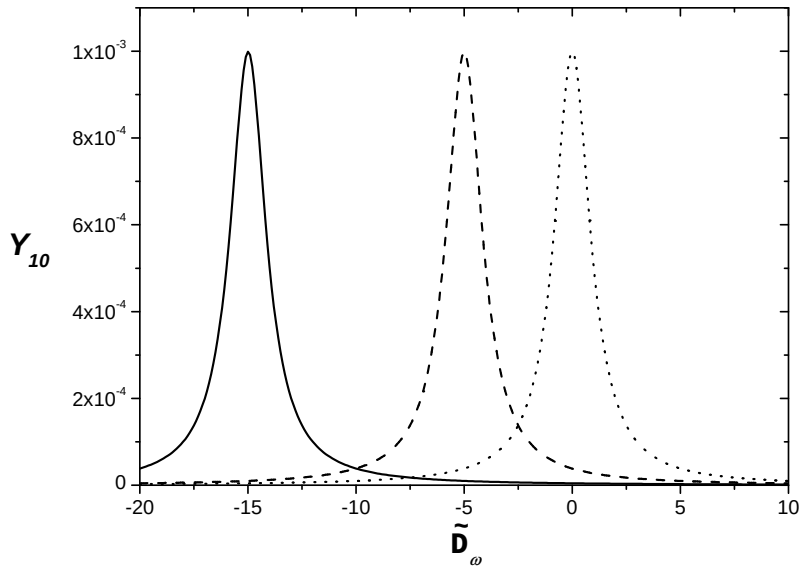

Figure 3.1: Imaginary part of the atomic coherence as a function of the probe field detuning for $\alpha_w = 0.01$, $b = 0.5$, $r = 0.1$ and $L = 0$ (dotted line), $L = 50$ (dashed line) and $L = 150$ (solid line).

Let us consider first parameters such that $\delta < 0$, e.g. take $\alpha_w^2 \ll b$. This implies that the third degree equation (3.5) has only one real solution. In Figure 3.1 this solution is plotted as a function of the probe field detuning, for different values of the local field corrections parameter, $L = 0$, $L = 50$ and $L = 150$. The rest of the parameters are $\alpha_w = 0.01$, $b = 0.5$ and $r = 0.1$. For $L = 0$, i.e., in the absence of local field effects (dotted line), the maximum of the curve is at $\tilde{\Delta}_w = 0$ as expected. However, for different values of the local field corrections parameter, $L = 50$ (dashed line) and $L = 150$ (solid line), a displacement of the resonance line toward negative values of the detuning, the so-called static Lorentz shift, is observed. This displacement in the amplification curve of the medium, is produced by the non-linear detuning, proportional to the population inversion (3.1), that appears in the optical Bloch equations (3.4) when local field corrections are considered. Inasmuch the probe field is weak enough, the population inversion

remains practically constant ($d \simeq 0.1$ for the set of the parameters used) for all the field detunings, and therefore the shift increases linearly with the parameter L.

We consider now the particular case in which $\delta > 0$, that can be obtained, for instance by imposing $\alpha_w^2 = b$. In this case, the discriminant reads:

$$\delta = -\frac{64L^2}{\alpha_w^2}\Big[5\tilde{\Delta}_w^4 + 16Lr\tilde{\Delta}_w^3 + (50 + 18L^2r^2)\tilde{\Delta}_w^2 + \\ +8Lr(L^2r^2 - 10)\tilde{\Delta}_w + L^4r^4 - 22L^2r^2 + 125\Big] \tag{3.8}$$

which can take positive values within a certain range of the probe field detuning parameter. In Figure 3.2 different curves representing δ vs. $\tilde{\Delta}_\omega$ for $b = 0.5$, $\alpha_w = \sqrt{b}$ and $r = 0.1$, and $L = 150$ (solid line), $L = 200$ (dashed line) and $L = 250$ (dotted line) are shown. One observe that the larger L, the greater becomes the region in which $\delta > 0$.

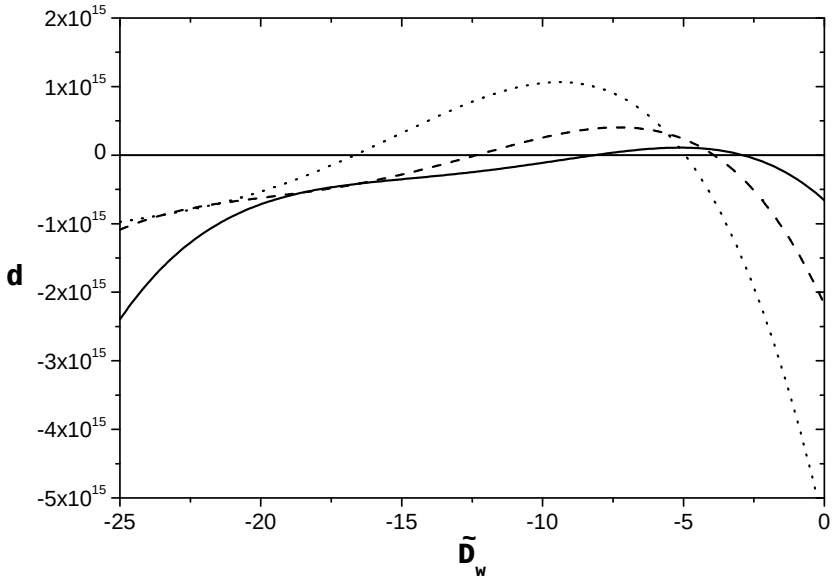

Figure 3.2: Discriminant of the equation (3.5) as a function of the probe field detuning for $b = 0.5$, $\alpha_w = \sqrt{b}$, $r = 0.1$, and $L = 150$ (solid line), $L = 200$ (dashed line) and $L = 250$ (dotted line).

The fact that δ could take positive values in a certain range of probe field detunings implies that equation (3.5) can exhibit three different real solutions within this range, depending on the value of L. In Figure 3.3 we plot the solutions of the equation (3.5) as a function of the probe field detuning parameter, for

$b = 0.5$, $\alpha_w = \sqrt{b}$, $r = 0.1$ and $L = 0$ (dashed line) and $L = 150$ (solid line). The steady-state solutions for the real part of the coherence, X_{10}, obtained from the solutions of the equation (3.5), are also plotted.

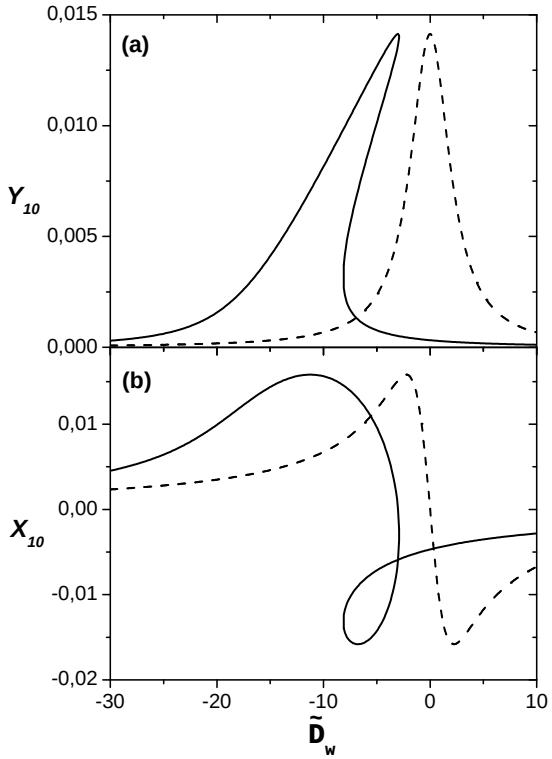

Figure 3.3: Real (a) and imaginary (b) part of the atomic coherence as a function of the field detuning for $b = 0.5$, $\alpha_w = \sqrt{b}$, $r = 0.1$, $L = 0$ (dashed line) and $L = 150$ (solid line).

As we can see in Figure 3.3(a) the effect of the local field corrections in this case is completely different from the situation represented in Figure 3.1 in which the Lorentzian profile is shifted as a whole. Here, the probe field is strong enough to modify the population distribution and thus we observe a non-linear displacement of the curve similar to that one finds when the lasing case is considered, in which the population inversion depends on the generated intensity (Subsection 3.1.2). In Figure 3.3(b), in the absence of local field corrections we observe the typical dispersion curve (dashed line), but when local field effects are considered (solid line) this curve is shifted toward negative values of the field detuning and a loop that connect the negative slope branch with the right side normal dispersion branch appears.

3.1.2 Dynamic Lorentz Shift

In contrast with the situation considered in the last subsection, in which the field is externally applied to the two-level medium, we consider here the case in which the field is generated by the active medium itself. In the lasing case, the population inversion depends on the generated intensity, giving rise to a population distribution as a function of the cavity detuning, which causes the dynamic Lorentz shift.

To study this situation, the optical Bloch equations (3.3) are considered. When the steady-state is reached, all the derivatives of (3.3) vanish and the stationary solutions can be obtained from the following equation for the imaginary part of the coherence:

$$0 = Y_{10}\left[A + BY_{10}^2 + CY_{10}^4\right] \tag{3.9}$$

where

$$A = b^2\tilde{\sigma}\left[\tilde{\sigma}(\tilde{\Delta}_c + Lr)^2 - (pr - \tilde{\sigma})(1+\tilde{\sigma})^2\right] \tag{3.10a}$$

$$B = 4pb\left[p(1+\tilde{\sigma})^2 - 2L\tilde{\sigma}(Lr + \tilde{\Delta}_c)\right] \tag{3.10b}$$

$$C = 16L^2p^2 \tag{3.10c}$$

On the one hand, equation (3.9) has a trivial solution, $Y_{10} = 0$, corresponding to a situation in which the laser is not emitting. For this non-lasing solution the amplitude of the field and the atomic coherence are zero, whereas the population inversion of the transition equals the pump rate r:

$$X_{10}^{(0)} = 0 \qquad Y_{10}^{(0)} = 0 \qquad \alpha^{(0)} = 0 \qquad d^{(0)} = r \tag{3.11}$$

On the other hand, (3.9) contains a biquadratic equation:

$$0 = \left[A + BY_{10}^2 + CY_{10}^4\right] \tag{3.12}$$

which has at most four mathematical solutions, $Y_{10} = \pm\sqrt{t_+},\ \pm\sqrt{t_-}$, where:

$$t_\pm = \frac{-B \pm \sqrt{B^2 - 4CA}}{2C} \tag{3.13}$$

However these four solutions correspond only to two different physical lasing states

due to the invariance of the equations under sign change in the amplitude of the field and the coherence terms. Therefore, the system exhibits always the trivial solution (3.11), and zero, one or two different lasing solutions depending on the parameters. From (3.13), it is easy to see that when $B^2 - 4CA \geqslant 0$ and $\sqrt{B^2 - 4CA} \geqslant B$ only one lasing solution, corresponding to $Y_{10} = \sqrt{t_+}$, exists. However, if $B^2 - 4CA > 0$ and $\sqrt{B^2 - 4CA} < |B|$ with $B < 0$, two different coexisting lasing steady-states solutions are found; $Y_{10} = \sqrt{t_+}$ and $Y_{10} = \sqrt{t_-}$. In any other case the Equation (3.12) has no real solution and therefore only the trivial solution (3.11) exists.

In order to determine the cavity detuning regions in which these lasing solutions exist the previous conditions are used. Imposing the condition $B^2 - 4CA \geqslant 0$ a higher limit of the cavity detuning for all lasing solutions is found:

$$\tilde{\Delta}_c \leqslant \frac{p^2\left(1+\tilde{\sigma}\right) - 4L^2\tilde{\sigma}^2}{4Lp\tilde{\sigma}} \equiv \tilde{\Delta}_{c2} \tag{3.14}$$

In addition, from the conditions $\sqrt{B^2 - 4CA} \geqslant B$ and $\sqrt{B^2 - 4CA} < |B|$, the lower cavity detuning limits in which the lasing solutions, $Y_{10} = \sqrt{t_+}$ and $Y_{10} = \sqrt{t_-}$ exist are, respectively:

$$\tilde{\Delta}_c \geqslant \frac{-Lr\sqrt{\tilde{\sigma}} - \left(1+\tilde{\sigma}\right)\sqrt{pr-\tilde{\sigma}}}{\sqrt{\tilde{\sigma}}} \equiv \tilde{\Delta}_{c0} \tag{3.15}$$

and

$$\tilde{\Delta}_c \geqslant \frac{-Lr\sqrt{\tilde{\sigma}} + \left(1+\tilde{\sigma}\right)\sqrt{pr-\tilde{\sigma}}}{\sqrt{\tilde{\sigma}}} \equiv \tilde{\Delta}_{c1} \tag{3.16}$$

From (3.14), (3.15) and (3.16), it can be seen that the system exhibits only one lasing solution in the cavity detuning range given by:

$$\tilde{\Delta}_{c0} \leqslant \tilde{\Delta}_c < \tilde{\Delta}_{c1} \tag{3.17}$$

and at:

$$\tilde{\Delta}_c = \tilde{\Delta}_{c2} \tag{3.18}$$

while two different lasing solutions can be found in the region:

$$\tilde{\Delta}_{c1} \leqslant \tilde{\Delta}_c < \tilde{\Delta}_{c2} \tag{3.19}$$

From these conditions, one can see that there is a minimum value of the local field corrections parameter, L_{th}, above which there are two steady-state lasing solutions. This critical value can be easily obtained imposing $\tilde{\Delta}_{c1} = \tilde{\Delta}_{c2}$:

$$L_{th} = \frac{p\,(1+\tilde{\sigma})}{2\sqrt{\tilde{\sigma}\,(pr-\tilde{\sigma})}} \tag{3.20}$$

Figure 3.4 shows the dependence of this threshold value with (a) r, (b) $\tilde{\sigma}$ and (c) p. By increasing r, with the rest of the parameters fixed, the threshold value of the local field corrections parameter, L_{th}, diminishes exponentially to zero, whereas for fixed values of p and r ($\tilde{\sigma}$ and r), the threshold exhibits a minimum at a given $\tilde{\sigma}$ (p).

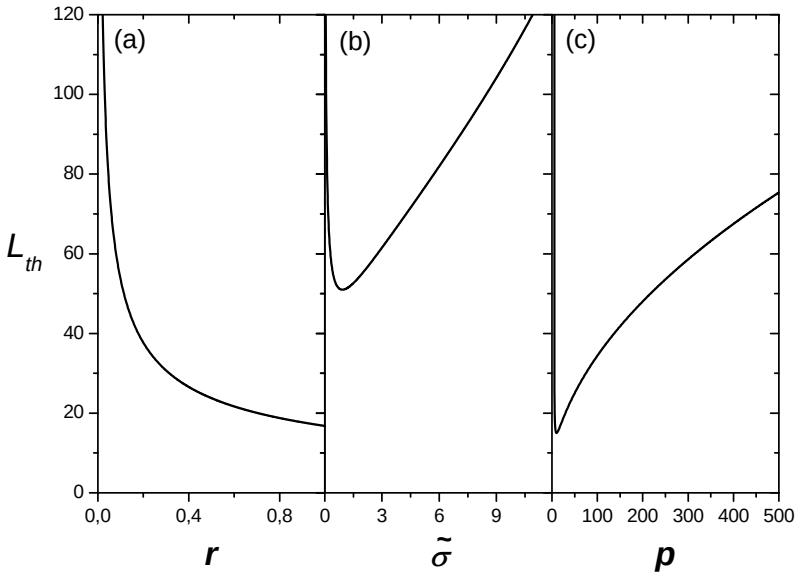

Figure 3.4: Threshold value of the local field corrections parameter as a function of (a) r with $\tilde{\sigma} = 0.5$ and $p = 250$, (b) $\tilde{\sigma}$ with $r = 0.1$ and $p = 250$, and (c) p with $\tilde{\sigma} = 0.5$ and $r = 0.1$.

The steady-state lasing solutions for the amplitude of the field, obtained from (3.3d) and (3.12), are shown in Figure 3.5 as a function of the cavity detuning, for $p = 250$, $\tilde{\sigma} = 0.5$, $b = 0.5$ and $r = 0.1$, and (a) $L = 0$ (dotted line), $L = 20$ (dashed line) and $L = L_{th}$ (solid line), where $L_{th} \simeq 53.6$ for the parameters used, and (b) $L = 0$ (dotted line) and $L = 150$ (dashed line). For $L = 0$ (dotted lines), i.e., in the absence of local field corrections, the curve is symmetric with the

maximum value at $\tilde{\Delta}_c = 0$ as expected. However, when the local field corrections parameter is increased, a clear displacement of the basis of the resonance lineshape is observed (Figure 3.5(a)), while the shift of the peak is rather small. This is due to the fact that the population distribution depends on the generated intensity: the highest intensity corresponds to the lowest population difference, in fact, $d \simeq 0$, and thus the shift ($\Delta^s = Ld$) of the peak at maximum intensity is practically zero. On the contrary, in the basis of the curve is where the population inversion is maximum, and hence the shift is larger. For the solid curve represented in Figure 3.5(b), the local field corrections parameter has been taken above the critical value, $L = 150 > L_{th}$ (the case $L = 0$ is shown again for comparison, represented by a dotted line). We observe that the magnitude of the shift in the resonance line is such that two different lasing solutions appear in the region between $\tilde{\Delta}_{c1}$ and $\tilde{\Delta}_{c2}$. In what follows, we will refer to those two solutions as the higher intensity (HI) lasing solution and the lower intensity (LI) lasing solution. Notice that the analytical limits for the coexistence of the different solutions, found in (3.19) and (3.17), evaluated for the parameters used in Figure 3.5(b) agree with the position of the vertical dashed lines in Figure 3.5(b): $\tilde{\Delta}_{c0} = -25.5$, $\tilde{\Delta}_{c1} = -4.5$ and $\tilde{\Delta}_{c2} = 1.6$.

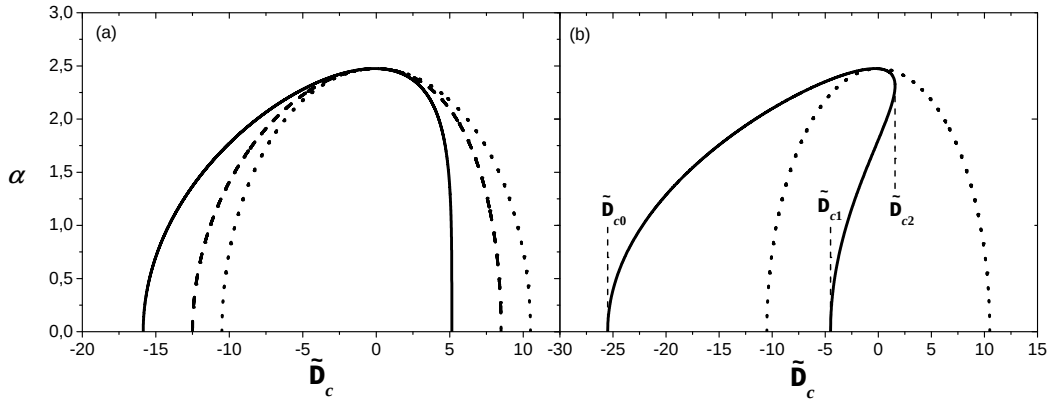

Figure 3.5: Lasing solutions for the amplitude of the generated field as a function of the cavity detuning for $p = 250$, $\tilde{\sigma} = 0.5$, $b = 0.5$, $r = 0.1$ and (a) $L = 0$ (dotted line), $L = 20$ (dashed line), $L = L_{th} \simeq 53.6$ (solid line); (b) $L = 0$ (dotted line), $L = 150$ (solid line). The vertical dashed lines in (b) indicate the limits of the region in which only one lasing solution exists ($\tilde{\Delta}_{c0} \leqslant \tilde{\Delta}_c < \tilde{\Delta}_{c1}$) and the region of coexistence the two lasing solutions ($\tilde{\Delta}_{c1} \leqslant \tilde{\Delta}_c < \tilde{\Delta}_{c2}$).

3.2 Linear Stability Analysis

In the previous section the coexistence of three different steady-state solutions in the presence of local field corrections has been reported. Here, we analyse the stability of these solutions by means of a linear stability analysis. As reported in what follows, the results of this analysis reveals that two of the three coexisting solutions (the non-lasing and the HI lasing solution) are always stable, while the third one (LI lasing solution) is always unstable, for any set of parameter values satisfying the coexistence conditions, (3.19), i.e., our system shows intrinsic optical bistability.

In order to perform the linear stability analysis we consider a general steady-state solution of the optical Bloch equations (3.3), $S = \left(\alpha^{(i)},\ d^{(i)},\ X_{10}^{(i)},\ Y_{10}^{(i)}\right)$ and apply a small perturbation of the form:

$$\alpha = \alpha^{(i)} + \delta\alpha e^{\lambda t} \tag{3.21a}$$

$$d = d^{(i)} + \delta d e^{\lambda t} \tag{3.21b}$$

$$X_{10} = X_{10}^{(i)} + \delta X_{10} e^{\lambda t} \tag{3.21c}$$

$$Y_{10} = Y_{10}^{(i)} + \delta Y_{10} e^{\lambda t} \tag{3.21d}$$

where λ is a complex exponential growth rate. Substitution of (3.21) into the full optical Bloch equations (3.3), up to first order, gives rise to the following set of equations:

$$\lambda\delta\alpha = -\tilde{\sigma}\delta\alpha - p\delta Y_{10} \tag{3.22a}$$

$$\lambda\delta d = 4\alpha^{(i)}\delta Y_{10} + 4Y_{10}^{(i)}\delta\alpha - b\delta d \tag{3.22b}$$

$$\begin{aligned}\lambda\delta X_{10} = &\left(\frac{X_{10}^{(i)}}{\alpha^{(i)}}p - Ld^{(i)} - \tilde{\Delta}_c\right)\delta Y_{10} - LY_{10}^{(i)}\delta d - \\ &- \left(1 + \frac{Y_{10}^{(i)}}{\alpha^{(i)}}p\right)\delta X_{10} + \frac{X_{10}^{(i)}Y_{10}^{(i)}}{(\alpha^{(i)})^2}p\delta\alpha\end{aligned} \tag{3.22c}$$

$$\begin{aligned}\lambda\delta Y_{10} = &\left(\alpha^{(i)} + LX_{10}^{(i)}\right)\delta d + \left(d^{(i)} - \left(\frac{X_{10}^{(i)}}{\alpha^{(i)}}\right)^2 p\right)\delta\alpha + \\ &+ \left(Ld^{(i)} + \tilde{\Delta}_c + \frac{2X_{10}^{(i)}}{\alpha^{(i)}}p\right)\delta X_{10}\end{aligned} \tag{3.22d}$$

These equations can be written as an eigenvalue problem:

$$(M - \lambda I)\delta\vec{v} = 0 \tag{3.23}$$

where I is the identity matrix, and we have defined the complex perturbed state vector:

$$\delta\vec{v} = \begin{pmatrix} \delta\alpha \\ \delta d \\ \delta X_{10} \\ \delta Y_{10} \end{pmatrix} \tag{3.24}$$

and the stability matrix, M:

$$M = \begin{pmatrix} -\tilde{\sigma} & 4Y_{10}^{(i)} & -\frac{X_{10}^{(i)}Y_{10}^{(i)}}{(\alpha^{(i)})^2}p & -d^{(i)} + \left(\frac{X_{10}^{(i)}}{\alpha^{(i)}}\right)^2 p \\ 0 & -b & LY_{10}^{(i)} & -LX_{10}^{(i)} - \alpha^{(i)} \\ 0 & 0 & \frac{Y_{10}^{(i)}}{\alpha^{(i)}}p - 1 & -Ld^{(i)} - \tilde{\Delta}_c - \frac{2X_{10}^{(i)}}{\alpha^{(i)}}p \\ -p & 4\alpha^{(i)} & Ld^{(i)} + \tilde{\Delta}_c + \frac{X_{10}^{(i)}}{\alpha^{(i)}}p & -1 \end{pmatrix} \tag{3.25}$$

The secular equation of the problem is given by:

$$\det(M - \lambda I) = 0 \tag{3.26}$$

In the following subsections, this equation will be solved for the case of the non-lasing (Subsection 3.2.1) and the lasing (Subsection 3.2.2) solutions, in order to find the stability conditions. From the perturbed steady-state solution defined in (3.21) it is easy to see that for $\mathrm{Re}(\lambda) < 0$ the perturbative terms decrease exponentially and thus a stable situation will be achieved, whereas for $\mathrm{Re}(\lambda) > 0$ these terms grow exponentially and the solution will be unstable. Considering the imaginary part of the eigenvalues one can see that in the case $\mathrm{Im}(\lambda) = 0$, only the real part contributes to the system dynamics and then an exponential behaviour is expected, while for $\mathrm{Im}(\lambda) \neq 0$ the complex perturbative terms add an oscillating component to the system dynamics.

3.2.1 Stability of the Trivial Solution

We consider first the trivial solution given by $X_{10}^{(0)} = Y_{10}^{(0)} = \alpha^{(0)} = 0$ and $d^{(0)} = r$. To solve the secular equation (3.26) we must avoid the divergence of the elements in the stability matrix (3.25) that contain $\alpha^{(0)} = 0$ in the denominator. For this purpose we assume that the variables X_{10} and Y_{10} have a linear behaviour with the field amplitude in the limit $\alpha \to 0$, i.e.:

$$X_{10} \simeq U(\tilde{\Delta}_c)\alpha \tag{3.27a}$$

$$Y_{10} \simeq V(\tilde{\Delta}_c)\alpha \tag{3.27b}$$

where $U(\tilde{\Delta}_c)$ and $V(\tilde{\Delta}_c)$ can be found from the Equations (3.3) at the steady-state. Therefore, the stability matrix (3.25) evaluated for the trivial solution (3.11) becomes:

$$M = \begin{pmatrix} -\tilde{\sigma} & 0 & UVp & -r + U^2 p \\ 0 & -b & 0 & 0 \\ 0 & 0 & Vp - 1 & -Lr - \tilde{\Delta}_c - 2Up \\ -p & 0 & Lr + \tilde{\Delta}_c + Up & -1 \end{pmatrix} \tag{3.28}$$

From Equation (3.26) and using (3.28), four different eigenvalues are found, $\lambda_1^{(tr)}$, $\lambda_2^{(tr)}$, $\lambda_3^{(tr)}$ and $\lambda_4^{(tr)}$, whose real and imaginary parts are plotted as a function of the cavity detuning (Figure 3.6), using the same parameter values as in Figure 3.5 for $L = 150$. On the one hand, the stability of the solution is determined by the sign of the real part of the eigenvalues. According to Figure 3.6(a) all the real parts are negative except for $\lambda_4^{(tr)}$ between the limits $\tilde{\Delta}_{c0} = -25.5$ and $\tilde{\Delta}_{c1} = -4.5$. Thus the non-lasing solution is unstable within this region and stable out of it. On the other hand, in the stable region, the dynamics of the system under small perturbations can be analysed by considering imaginary part of the eigenvalue with smaller absolute real part. In this case, the eigenvalue with minimum absolute real part corresponds to $\lambda_3^{(tr)}$ for the most of cavity detuning values, but also to $\lambda_4^{(tr)}$ in a small range near $\tilde{\Delta}_{c0}$ and $\tilde{\Delta}_{c1}$. In both cases, because of their null imaginary part the system should exhibit an exponential behaviour.

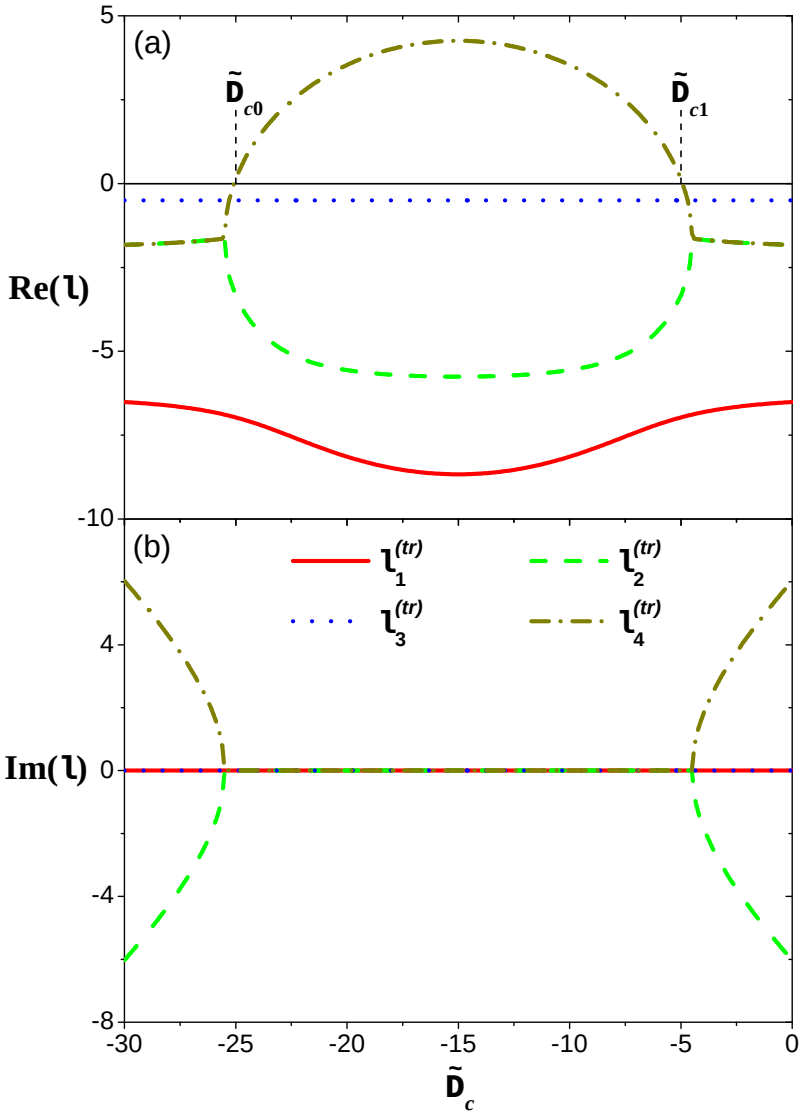

Figure 3.6: Real (a) and imaginary (b) parts of the eigenvalues of the secular equation (3.26) for the trivial solution versus the cavity detuning, for $L = 150$. The other parameter values are the same as in Figure 3.5.

3.2.2 Stability of the Lasing Solutions

Considering now the two lasing solutions and using the same parameters as in Figure 3.5 for $L = 150$, the eigenvalue equation (3.23) is solved again. Four different eigenvalues are found for each solution: $\lambda_1^{(HI)}$, $\lambda_2^{(HI)}$, $\lambda_3^{(HI)}$ and $\lambda_4^{(HI)}$ corresponding to the HI lasing solution, and $\lambda_1^{(LI)}$, $\lambda_2^{(LI)}$, $\lambda_3^{(LI)}$ and $\lambda_4^{(LI)}$ for the LI lasing solution.

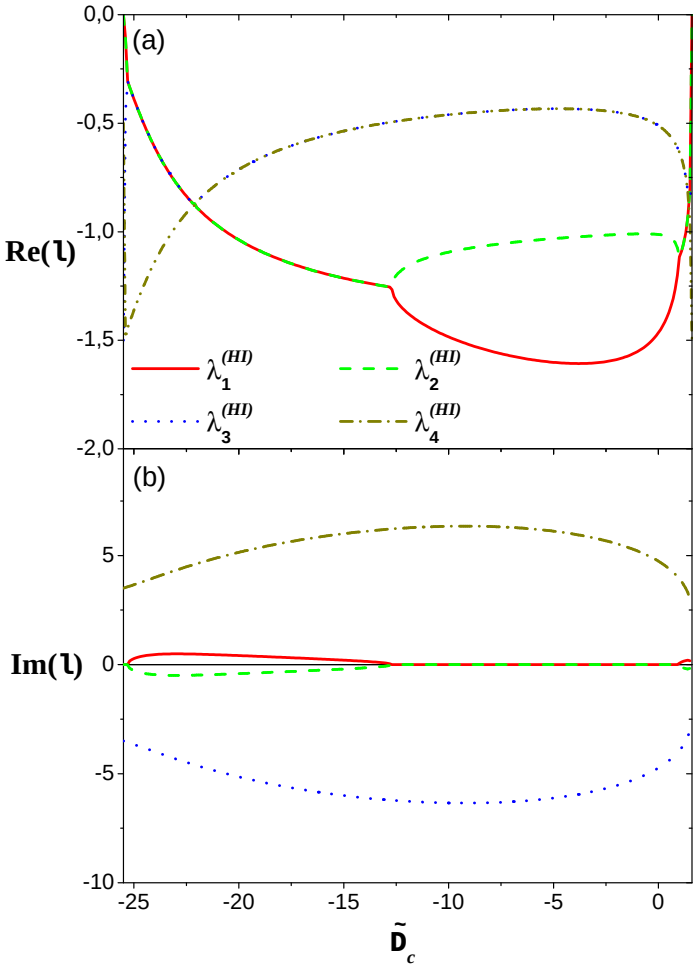

Figure 3.7: Real (a) and imaginary (b) parts of the eigenvalues of the secular equation (3.26) for the higher intensity non-trivial solution versus the cavity detuning, for $L = 150$. The other parameters are as in Figure 3.5.

The dependence of the real and imaginary parts of the eigenvalues $\lambda_1^{(HI)}$, $\lambda_2^{(HI)}$, $\lambda_3^{(HI)}$ and $\lambda_4^{(HI)}$ versus the cavity detuning is shown in Figure 3.7. The curves of

the real part of the eigenvalues (Figure 3.7(a)), clearly show that all the eigenvalues have negative real part, and thus the HI lasing solution is stable for all the studied range of cavity detuning. In addition, since the eigenvalues with real part closer to zero have non-null imaginary parts, the system is expected to perform oscillations when it reaches the steady-state, at the corresponding frequency $\omega = \mathrm{Im}\,(\lambda)$.

The real and imaginary parts of the eigenvalues corresponding to the LI lasing solution ($\lambda_1^{(LI)}$, $\lambda_2^{(LI)}$, $\lambda_3^{(LI)}$ and $\lambda_4^{(LI)}$) are plotted in Figure 3.8 as a function of the cavity detuning. Since $\mathrm{Re}(\lambda_4^{(LI)})$ is positive in the whole range of cavity detunings this solution is unstable.

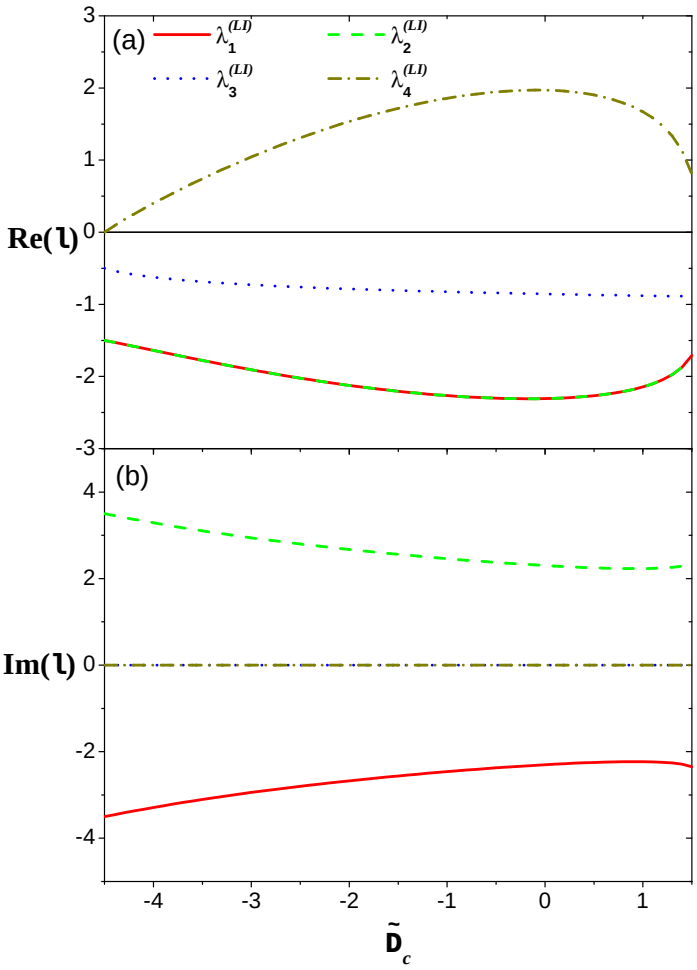

Figure 3.8: Real (a) and imaginary (b) parts of the eigenvalues of the secular equation (3.26) for the lower intensity lasing solution versus the cavity detuning, for $L = 150$. The other parameter values are the same as in Figure 3.5.

The results of our linear stability analysis are summarized in Figure 3.9(a), which shows the solutions for the amplitude of the generated field versus the cavity detuning parameter, $\tilde{\Delta}_c$. The stable solutions are represented with solid lines, while the unstable ones are represented with dotted lines. The vertical dashed lines, as in Figure 3.5(b), mark the limits of existence of the lasing solutions. These limits, given by (3.17) and (3.19), are represented in Figure 3.9(b) as a function of the local field parameter L. The vertical dashed line indicates the threshold value, L_{th}, given by (3.20), above which bistability occurs and the area determined by $\tilde{\Delta}_{c1}$ and $\tilde{\Delta}_{c2}$ (gray region) corresponds to the bistability region.

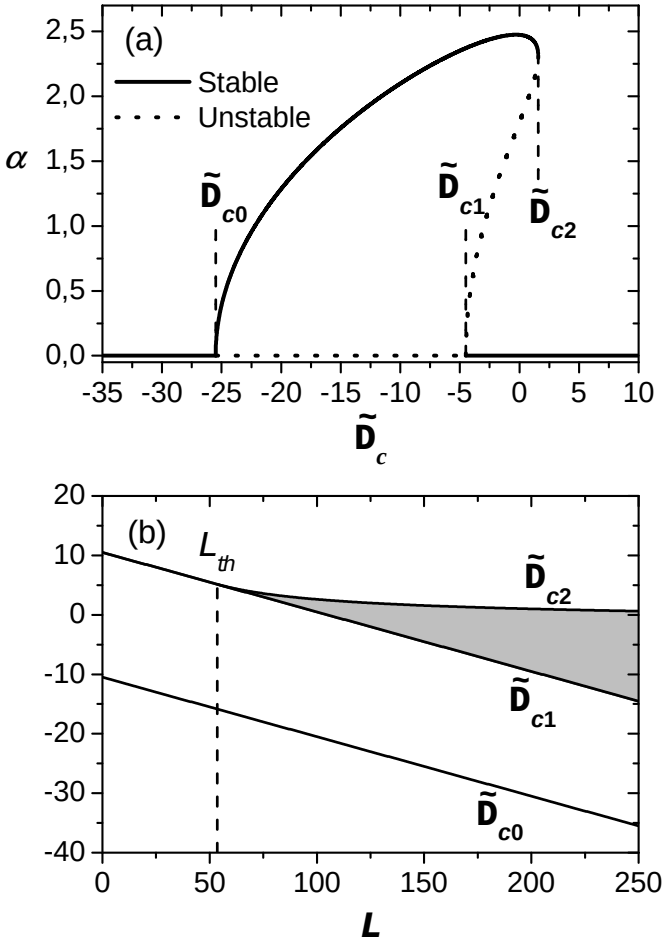

Figure 3.9: (a) Stable (solid line) and unstable (dotted line) solutions for the amplitude of the field as a function of the cavity detuning for $p = 250$, $\tilde{\sigma} = 0.5$, $b = 0.5$, $r = 0.1$ and $L = 150$. (b) Limits of the lasing solutions as a function of the local field corrections parameter, L, for $p = 250$, $\tilde{\sigma} = 0.5$ and $r = 0.1$.

The analytical results obtained in this section have been contrasted with the evolution of the amplitude of the field, obtained from the numerical integration of the optical Bloch equations (2.58). This numerical integration has been performed using a Runge-Kutta-Fehlberg routine. The analytical solutions shown in Figure 3.9(a) agree with the steady-state solutions obtained numerically. In addition, the dynamics exhibited by the variables α, d, X_{10} and Y_{10} in the numerical calculations is in good agreement with the predictions done from figures 3.6(b) and 3.7(b).

In conclusion, we have shown that the two-level lasing system under investigation exhibit coexistence of two stable steady-state solutions, i.e., bistability is achieved in the stationary regime for a certain region of the cavity detuning when the local field corrections parameter, L, is above a threshold value, L_{th}.

4

Effects of the Doppler Broadening in the Intrinsic Optical Bistability

This chapter deals with the inclusion of the Doppler effect in the studied two-level gas laser in the presence of local field corrections. The Doppler effect, which is due to the atomic motion of the atoms, is introduced in Section 4.1 and a theoretical description of the Doppler broadening and the hole burning phenomenon, both caused by the Doppler effect, is presented. In Section 4.2 the optical Bloch equations derived in Chapter 2 are generalized to include the Doppler broadening. Next, the numerical results obtained by integration of the generalized optical Bloch equations are presented in Section 4.3. The effect of the local field corrections in the hole burned in the population distribution, due to the saturation of the transition, is investigated first for cases in which the local field corrections are below the threshold value L_{th}. For values of L above the threshold, in which the system exhibits intrinsic optical bistability, the behaviour of the amplitude of the field as a function of the Doppler width is also analysed, and interpreted by studying the population inversion and gain distributions over velocity classes for different Doppler widths and local field corrections parameter values. Finally, in Section 4.4, we discuss the possibility of implementing the reported phenomena considering realistic parameters.

4.1 Introduction

4.1.1 Doppler Broadening

Up to now, we have considered only the homogeneous broadening case, i.e., it has been considered that all the atoms "see" the external field with the same frequency and therefore, the detuning is independent of the atom under consideration. Nevertheless, in vapor cells at finite temperature, the atoms are in thermal equilibrium and they move randomly in all directions with a velocity interval given by the temperature of the gas, e.g., typical average atomic velocities in vapor cell at room temperature range between 10^2-10^3 m/s. Such atomic motion implies that, in general, when dealing with an optical transition, the Doppler effect has to be taken into account. This means that an atom with velocity $\vec{v}$ "sees" a light field of frequency ω_n, with a shifted frequency given by:

$$\omega^d(\vec{v}) = \omega_n \left[1 - \frac{\vec{v}}{c}\vec{u}\right] \tag{4.1}$$

where $\vec{u}$ is the unitary vector in the direction of the propagation of the field and c is the speed of light in vacuum. The difference between the nominal frequency of the field and the shifted frequency, $\Delta^d \equiv \frac{\omega_n \vec{v}}{c}\vec{u}$, is named Doppler shift.

In a vapor cell in thermal equilibrium, all directions of the moving atoms are equiprobable, i.e., the velocity distribution of the particles is isotropic. Therefore, the velocity projection of the particles in a given direction (the propagation direction of the laser field) can be modelized by a Maxwell distribution:

$$P(v) = \frac{1}{\eta\sqrt{\pi}} \exp\left(-v^2/\eta^2\right) \tag{4.2}$$

where $\eta = \sqrt{2K_BT/m}$ is the most probable velocity, with K_B the Boltzmann's constant, T the temperature, and m the mass of the atom. Accordingly, the velocity distribution for the atomic density, $N(v)$, and for the population inversion, $d(v)$, read:

$$N(v) = \frac{N_T}{\eta\sqrt{\pi}} \exp\left(-v^2/\eta^2\right) \tag{4.3a}$$

$$d(v) = \frac{d_T}{\eta\sqrt{\pi}} \exp\left(-v^2/\eta^2\right) \tag{4.3b}$$

where N_T is the total density of atoms and d_T is the total population inversion.

Then, the spectral-line shape of the whole set of particles $S(\omega)$ is determined by the line-shape envelop of an individual particle with the Doppler-shift distribution:

$$S(\omega) = \int a_v(\omega, v)P(v)dv \tag{4.4}$$

where $a_v(\omega, v)$ is the spectral line of a single particle in the presence of Doppler effect. Considering the Maxwellian velocity distribution of the particles (4.2), the total full width at half maximum (FWHM) of the spectral line due to the Doppler effect $\Delta\omega_d$ is given by:

$$\Delta\omega_d = 2\sqrt{\ln 2}\frac{\eta}{c}\omega_n \tag{4.5}$$

In general, the presence of Doppler effect in optical systems is not desirable since it causes an important broadening of the resonance line. For instance, in a vapor cell at room temperature, the Doppler width of an optical transition, e.g., ~ 1 GHz, is considerably larger than the homogeneous width of an electric dipole allowed transition, e.g., ~ 10 MHz. The broadening of the resonance line causes that the number of atoms that contribute to the gain of the laser, i.e., the atoms that are resonant with the cavity frequency, diminishes when the Doppler width increases. This leads in a two-level lasing system to a progressive decrease of the field amplitude with increasing Doppler width and eventually, in our case, to a loss of bistability above a certain value of the Doppler width, as we will see in Subsection 4.3.2.

4.1.2 Hole Burning

A Doppler-broadened spectral line is basically the convolution of a large number of homogeneous broadened spectral lines, corresponding to individual atoms/molecules with different velocities. Thus, when the spectral line is Doppler broadened, the electromagnetic (e.m.) field interacts only with atoms with which it is nearly in resonance. For instance, consider a single mode of a travelling plane wave of the form:

$$E(\vec{r}, t) = E_n(t)\cos(\omega_n t - \vec{K}_n\vec{r} + \phi(t)) \tag{4.6}$$

where E_n and $\phi(t)$ are the amplitude and the phase of the field, respectively, $\omega_n + \dot{\phi}(t)$ is the oscillation frequency of the field and, $K_n = \omega_n/c$ the wave number with c the speed of light in vacuum. Then, the travelling wave interacts only with

atoms at the resonance frequency $\omega_n + \dot{\phi} = \omega_{ab} + \vec{K}_n\vec{v}$, being ω_{ab} the frequency of the atomic transition, within the spectral range of the homogeneous width, 2γ, where γ is the spontaneous emission decay rate of both the upper and the lower levels of the two-level system (Figure 2.1(b)). Then, the resonance condition reads:

$$\left|\omega_{ab} - (\omega_n + \dot{\phi}) + K_n v\right| \leq 2\gamma \tag{4.7}$$

In other words, only the atoms with velocity within the range:

$$v \leq \frac{c}{\omega_n}\left|2\gamma + \omega_{ab} - (\omega_n + \dot{\phi})\right| \tag{4.8}$$

will interact with the e.m. field.

So the e.m. field can change the state of this small part of atoms and discriminate them from the rest of the atoms, with velocities do not satisfying the resonance condition (4.8). If the intensity of the light field is sufficient to transfer a considerable part of the atoms to the excited state of the transition, the equilibrium population distribution of velocities, $d(v)$, can be altered. Consider the probability W_{ab} of absorption of an atom with velocity $\vec{v}$, under the influence of the travelling wave (4.6) [37]:

$$W_{ab}(v) = \frac{G}{2}\frac{\gamma^2}{(\Delta + K_n v)^2 + \gamma^2(1+G)} \tag{4.9}$$

where $\Delta = \omega_{ab} - (\omega_n + \dot{\phi})$ is the detuning of the field, $G = (\mu_{ab}E_n/\hbar\gamma)^2$ denotes the saturation parameter of the transition, μ_{ab} is the matrix element of the dipole moment of the transition and $\hbar$ is the Planck's constant. The peak of this Lorentzian function is centered at the resonance velocity:

$$K_n v_{res} = -\Delta \tag{4.10}$$

and its width reads:

$$\Delta W_{ab} = 2\gamma\sqrt{1+G} \tag{4.11}$$

Then, since the probability of transition of the atoms (4.9) is determined by the saturation parameter G and by the Doppler shift, the lower and the upper level develops a shortage and an excess, respectively, of atoms with velocities that fulfill the resonance condition (4.8). Therefore, the population inversion distribution in

the presence of a saturating field is modified from the Maxwellian distribution $d(v)$, given by (4.3b), as follows [37]:

$$d'(v) = d(v)\,[1 - 2W_{ab}(v)] \tag{4.12}$$

The three terms appearing in (4.12) are plotted schematically in Figure 4.1 as a function of the Doppler shift, $K_n v$. As we see in Figure 4.1(a), the term $[1 - 2W_{ab}(v)]$ exhibits a hole centered at the resonance velocity (4.10) (vertical line). The depth of the hole is determined by the saturation parameter G, and its width depends on the homogeneous width and the saturation parameter according to (4.11). The population distribution of the projections of atomic velocities in the laser-beam direction (4.12) in the presence, $d'(v)$, and in the absence, $d(v)$, of saturation are depicted in Figure 4.1(b) with solid and dashed lines, respectively. In this figure we show how the saturation of the transition for the resonant atoms plotted in Figure 4.1(a) modifies the population inversion $d(v)$ (dashed line), giving rise to the hole in the profile of $d'(v)$ (solid curve). The appearance of such a narrow structure inside the Doppler profile due to the saturation of the transition is known as hole burning, and it can only be observed with monochromatic, collimated and relatively intense radiation, i.e., with a saturating laser field.

Finally, note that the hole burned in the population distribution $d'(v)$ (solid line in Figure 4.1(b)) is centered near the resonance velocity (vertical line), but does not coincide exactly with this value (see Figure 4.1(a)). This discrepancy is due to the fact that when the distribution of atomic velocities is taken into account, the minimum of the population distribution does not correspond to the minimum of the term $[1 - 2W_{ab}(v)]$ but to a value which, in general, tends to move away from the maximum of the Maxwell distribution, i.e., from the central velocity. This displacement depends on the relative position of the resonance velocity in the Maxwell distribution. If the hole plotted in Figure 4.1(a) is in a range of velocities corresponding to a flat region of the Maxwell distribution $d(v)$ the displacement of the hole position in the population distribution $d'(v)$ will be small, whereas if the resonance velocity is in a high slope region of $d(v)$ the displacement of the hole burned in $d'(v)$ will be larger. For the same reason, the width of the hole does not exactly match with the width of the curve of Figure 4.1(a). Therefore these discrepancies will be only appreciable in case in which the Doppler width is similar to the width of the hole, i.e., the homogeneous width. For Doppler widths much larger, the values of the Maxwellian distribution which modify the hole are

almost constant, and thus the shape and the position of the hole does not change.

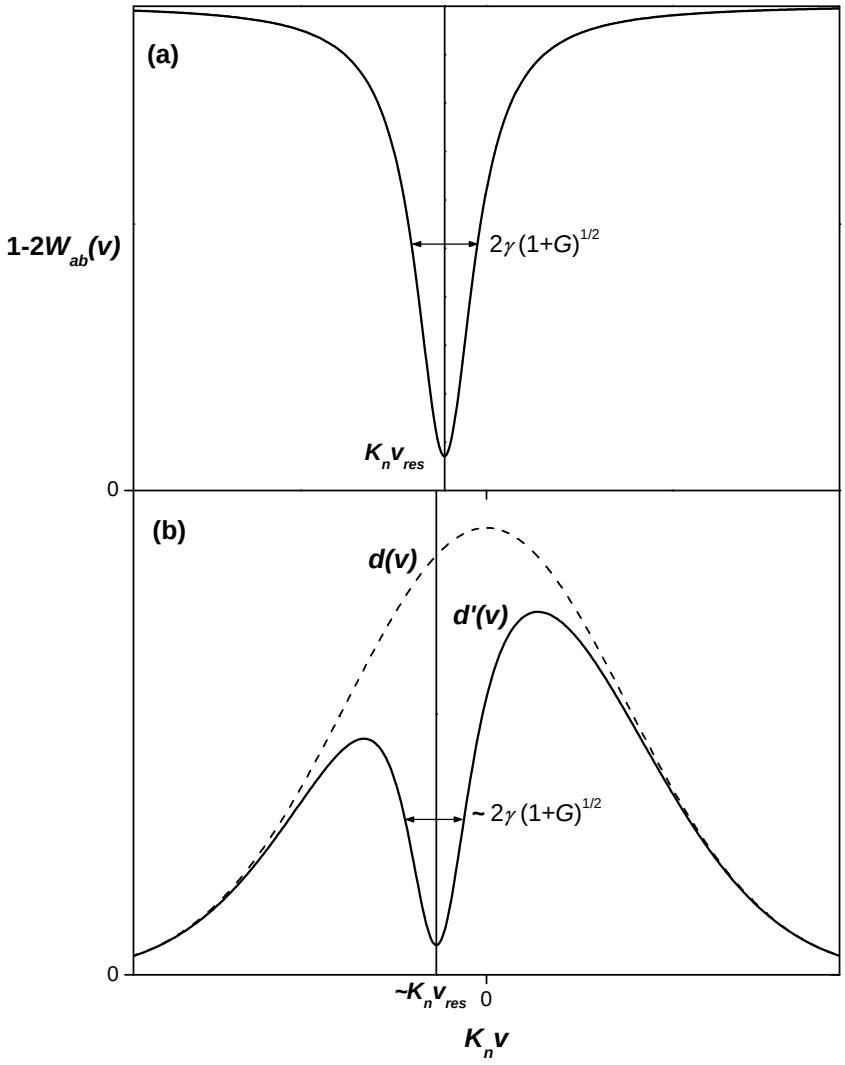

Figure 4.1: (a) Coefficient $[1 - 2W_{ab}(v)]$ as a function of the Doppler shift. (b) Schematic distribution of the population inversion as a function of the Doppler shift with (solid line) and without (dashed line) saturation of the transition.

4.2 Equations in the presence of Doppler broadening

The aim of this work is to study the effect of the Doppler broadening in the optical bistability induced by the local field corrections. Therefore, in the following we

will take into account the motion of the two-level atoms placed in the vapor cell at finite temperature, and we will introduce the necessary modifications into the normalized optical Bloch equations (2.58), derived in Chapter 2, to describe the system. The normalization used in what follows is the same as defined in (2.56) (Subsection 2.5.1). Consider an atom with a velocity projection in the direction of the propagation of the field, v. From (4.1) it is immediately seen that the atom exhibits a velocity dependent detuning $\tilde{\Delta}_c^d(v)$ given by:

$$\tilde{\Delta}_c^d(v) = \tilde{\Delta}_c + \Omega v \quad , \quad \Omega = \frac{\omega_n}{\gamma_\perp c} \tag{4.13}$$

where $\tilde{\Delta}_c = (\omega_{ab} - \omega_n)/\gamma_\perp$ is the normalized cavity field detuning, ω_{ab} is the frequency of the atomic transition, ω_n is the nominal frequency of the field, $\gamma_\perp$ is the coherence decay rate used for the normalization and c is the speed of light in vacuum. As a consequence of this velocity dependence in the frequency, the population inversion and the atomic coherence become velocity dependent and one must perform an integration in the field equation (2.58c) and in the evolution equation of the atomic coherence (2.58b) to obtain the contribution of all the atoms to the field and to the local field corrections, respectively. Then the optical Bloch equations (2.58) read:

$$\dot{\tilde{\alpha}} = -\tilde{\sigma}\tilde{\alpha} + ip \int \rho_{10}(v)^* dv \tag{4.14a}$$

$$\dot{\rho}_{10}(v) = i\tilde{\alpha}^* d(v) - \left[1 - i\left(\tilde{\Delta}_c^d(v) + L \int d(v)dv\right)\right] \rho_{10}(v) \tag{4.14b}$$

$$\dot{d}(v) = b\left[r(v) - d(v)\right] - 4\,\mathrm{Im}\left[\tilde{\alpha}\rho_{10}\left(v\right)\right] \tag{4.14c}$$

where $\tilde{\alpha}$ is the complex amplitude of the field, $\rho_{10}(v)$ and $d(v)$ are the atomic coherence and the population inversion, respectively, for an atom with a given velocity v in the propagation direction of the field, $\tilde{\sigma}$ is the damping rate of the field due to cavity losses, $p = N_T/N_0$ is the ratio between the total density of atoms N_T and a reference value N_0, $L = \gamma_\perp p/3\omega_n$ is the normalized local field corrections parameter and b is the decay rate of the population inversion. The parameter $r(v)$ is the pumping rate, which becomes velocity dependent since we consider an open two-level system and therefore the pumping rate for each atom depends on the number of atoms with the same velocity. Then, the total pumping rate can be defined as $r = \int r(v)dv$.

Since the atoms of the medium are in a vapor cell we will take the standard

Maxwellian velocity distribution given by (4.3b), characterized by the full width at half maximum (FWHM) of the absorption profile of a purely Doppler-broadened vapor (4.5), which reads in normalized form:

$$\tilde{\Delta}\omega_d = 2\Omega\sqrt{\ln 2}\eta \tag{4.15}$$

To obtain the time evolution of the system we have integrated the equations (4.14a), (4.14b) and (4.14c) by using a Runge-Kutta-Fehlberg routine. The velocity distribution is splitted into discrete groups or velocity classes with all the atoms belonging to a given group taken as moving with the same velocity. In all cases shown below we have considered a velocity distribution with more than 99.7% of the atoms and a large enough number of velocity classes to assure the convergence of the results.

4.3 Results

4.3.1 Local Field Corrections dependence in the Hole Burning

We have seen (Section 4.1) that, in relatively intense lasers and in the presence of the Doppler effect, the e.m. field saturates the transition of atoms belonging to a certain range of velocities. This effect leads to a Lorentzian-shaped hole in the population inversion distribution as the one shown in Figure 4.1(b), phenomenon known as hole burning. This hole is centered at the resonance velocity and, whereas its width depends on both the homogeneous width and the saturation parameter, i.e., the intensity of the field, its depth depends only on the latter. On the other hand, we have shown in the previous chapter that the inclusion of the local field corrections in the optical Bloch equations gives rise to a term proportional to the population inversion, $\Delta^s = Ld$, which can be interpreted as a non-linear detuning, and it is responsible for the static and the dynamic Lorentz shifts, and for the intrinsic optical bistability when the parameter L is above a threshold value ($L > L_{th}$).

In the Doppler broadened case and in the presence of local field corrections the effective detuning in the coherence equation (4.14b), $\tilde{\Delta}_c^d(v) + Ld_T$, has two different contributions: one contribution due to the Doppler effect, Ωv, and the other due to the local field corrections, Ld_T, where $d_T = \int d(v)dv$. Consequently,

the resonance condition for the atomic velocities takes the form:

$$\left|\tilde{\Delta}^d(v) + Ld_T\right| \leq 2b \tag{4.16}$$

where $\tilde{\Delta}^d(v) = \tilde{\Delta}_c^d(v) - \dot{\phi}/\gamma_\perp$ is the field detuning, $\dot{\phi}$ is the dispersion of the medium, $\gamma_\perp$ is the transverse decay rate used for the normalization and $b = \gamma/\gamma_\perp$ is the decay rate of the population inversion. This implies, that the position of the hole burned in the population distribution depends now also on the parameter L and on the total population inversion, d_T:

$$\Omega v_{res} = \dot{\phi}/\gamma_\perp - \tilde{\Delta}_c - Ld_T \tag{4.17}$$

To study the dependence of the hole burning position on the local field corrections parameter, we consider values of L below the threshold value for bistability. The population distribution at the steady-state is plotted in Figure 4.2(a) as a function of the normalized Doppler shift Ωv, for $L = 0$ (solid line), $L = 20$ (dashed line) and $L = 40$ (dotted line). The Doppler width is fixed at $\tilde{\Delta}\omega_d = 10$, value for which we can assure that the hole position corresponds to the resonance velocity (4.17) (see discussion of Figure 4.1), and the rest of the parameters are $\tilde{\Delta}_c = 0$, $\tilde{\sigma} = 0.5$, $b = 0.5$, $p = 250$ and $r = 0.1$. Since we have fixed $\tilde{\Delta}_c = 0$, in the absence of local field corrections (solid line) the population distribution is symmetric and centered at the position of the hole ($\Omega v = 0$). However, increasing L, we observe a displacement of the hole position towards negative velocities. Note that the width of the hole as well as its depth, which depends on the population decay rate b and on the saturation parameter $G = (2\tilde{\alpha}/b)^2$, remain constant when L varies. As we can appreciate in Figure 4.2(b), in which the hole position (green circles), given by the resonance velocity Ωv_{res}, the Lorentz shift Ld_T (red squares) and the dispersive effects $\dot{\phi}/\gamma_\perp$ (blue crosses) are plotted as a function of the local field corrections parameter, the displacement of the hole is linear with the parameter L and satisfies (4.17). In addition, it is important to note that this linear behaviour is exhibited not only for this value of the Doppler width $\tilde{\Delta}\omega_d = 10$, but also for a wide range of values large enough to ensure that the hole position corresponds to the resonance velocity (see discussion of Figure 4.1).

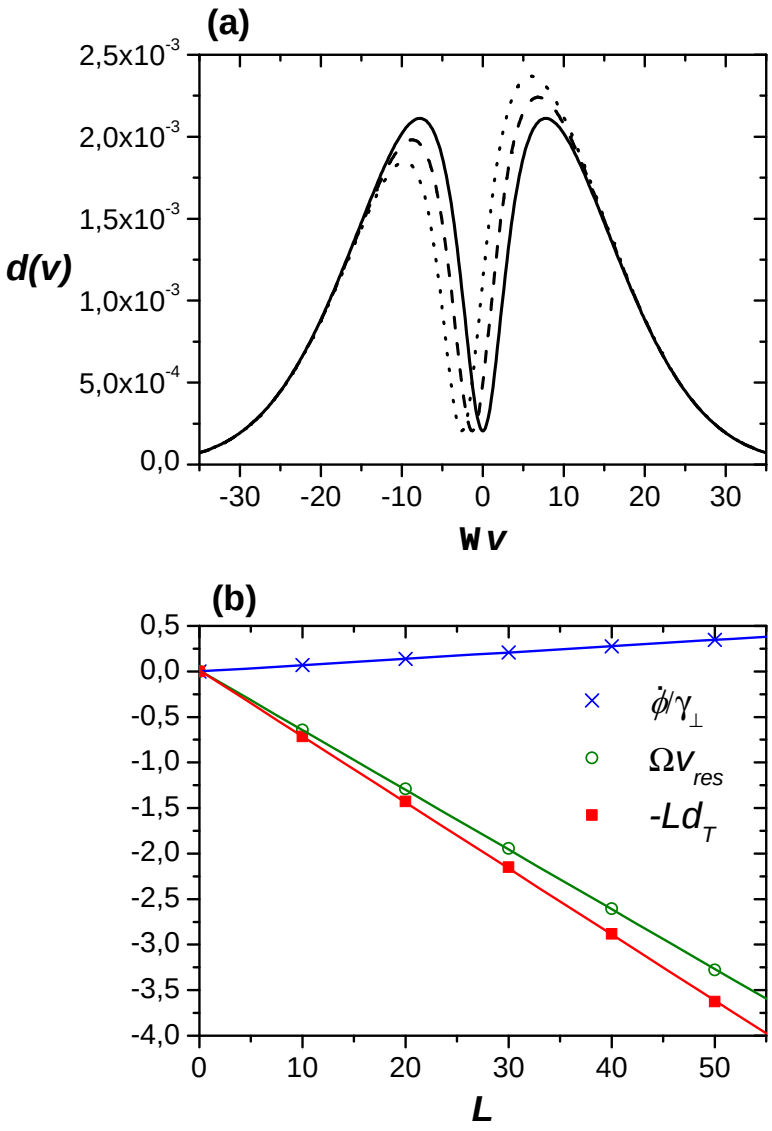

Figure 4.2: (a) Population inversion distribution as a function of the Doppler shift for $L = 0$ (solid line), $L = 20$ (dashed line), $L = 40$ (dotted line), $\tilde{\Delta}_c = 0$, $p = 250$, $\tilde{\sigma} = 0.5$, $b = 0.5$, $r = 0.1$ and $\tilde{\Delta}\omega_d = 10$ and (b) hole burning position (green circles), Lorentz shift (red squares) and dispersion of the medium (blue crosses) for the same parameters.

This linearity in the position of the hole comes from the fact that for the considered values of L ($L < L_{th}$), the amplitude of the field, and hence the total population inversion, remain practically constant with respect the local filed corrections parameter, and therefore the Lorentz shift Ld_T only varies with L. To show that the field does not change in the range of L's considered, we plot in Figure 4.3 the field amplitude as a function of the Doppler width $\tilde{\Delta}\omega_d$, for the same parameters as in Figure 4.2 and $L = 0$ (red line), $L = 10$ (green line), $L = 20$ (blue line), $L = 30$ (dark yellow line), $L = 40$ (brown line) and $L = 50$ (dark green line). It is important to remark that the values of L's considered in this subsection are smaller than the threshold value $L_{th} \simeq 53.6$, above which the system exhibits bistability. As we will see in the next subsection, inasmuch the value of L increases, the intensity of the field decrease, leading to an important variation of the total population inversion, and therefore the linearity in the hole position with L vanishes.

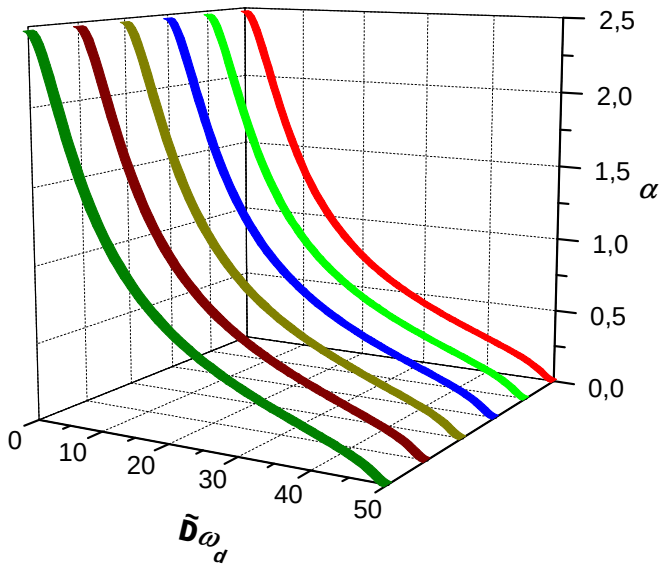

Figure 4.3: Amplitude of the generated field as a function of the Doppler width for $L = 0$ (red line), $L = 10$ (green line), $L = 20$ (blue line), $L = 30$ (dark yellow line), $L = 40$ (brown line), $L = 50$ (dark green line), and the rest of the parameters as in Figure 4.2.

In addition to the dependence of the hole burning position with the parameter L, the hole exhibits also an extra displacement when the Doppler width is changed. Figure 4.4 shows the population inversion distribution for Doppler widths $\tilde{\Delta}\omega_d = 5$ (solid line), $\tilde{\Delta}\omega_d = 10$ (dashed line) and $\tilde{\Delta}\omega_d = 15$ (dotted line). The rest of the parameters are the same as in Figure 4.2 with the local field corrections parameter fixed at $L = 40$. Since the amplitude of the field decreases with the Doppler width, the total population inversion, as well as the Lorentz shift Ld_T, increases. As a consequence, the hole position moves towards negative values of the normalized velocity range. In Figure 4.4, in addition to the displacement of the hole, one can appreciate an increase of its minimum, i.e., the maximum saturation value for the population inversion, due to the attenuation of the amplitude of the field. Thus, the dependence of the amplitude of the field on the total population inversion causes that the theoretical hole position, i.e., the position of the resonance velocity, as a function of the Doppler width exhibits a similar profile that the one shown by the amplitude of the field (see Figures 4.3 and 4.5). Note that in the limit of large Doppler widths such that the field is nearly zero, the theoretical position of the hole remains constant because of the total population inversion equals the pump rate. However, since the generated field is so weak, the saturation of the transition is practically zero, and therefore the hole disappears.

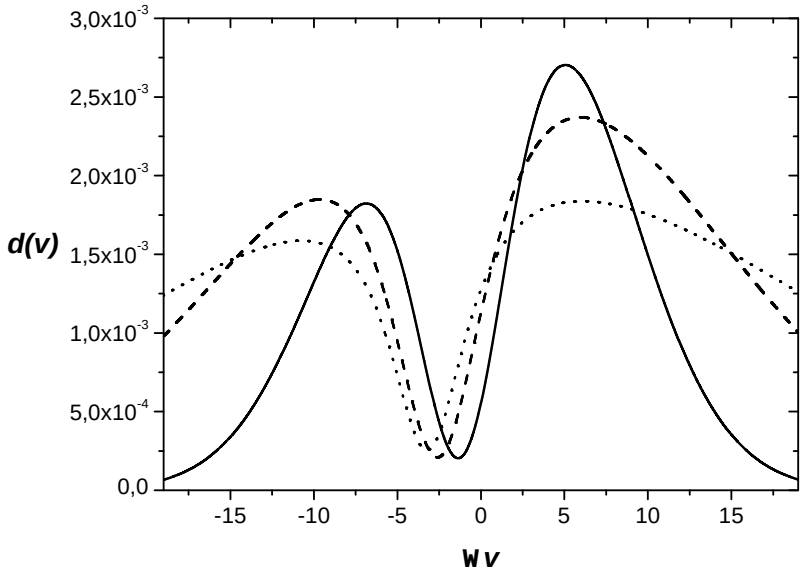

Figure 4.4: Population inversion distribution as a function of the Doppler shift for $\tilde{\Delta}\omega_d = 5$ (solid line), $\tilde{\Delta}\omega_d = 10$ (dashed line), $\tilde{\Delta}\omega_d = 15$ (dotted line), $L = 40$, and the rest of the parameters as in Figure 4.2.

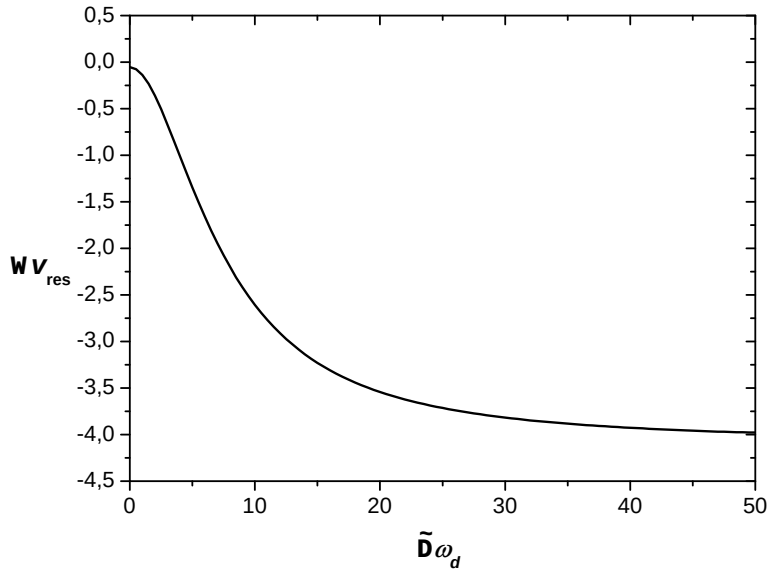

Figure 4.5: Resonance Doppler shift as a function of the Doppler width for $L = 40$ and the rest of the parameters as in Figure 4.2.

4.3.2 Bistability in the Presence of Doppler Broadening

In the last subsection we have seen that the inclusion of the local field corrections into the optical Bloch equations of a Doppler broadened medium changes the resonance condition of the atomic transition (4.16). The difference in the condition is the Lorentz shift ($\Delta^s = Ld_T$) and it has been shown that, for values of the local field corrections parameter below the threshold value Lth, the effect produced by this term is only a linear displacement of the hole burned in the population distribution due to the saturation of the transition.

In the following we investigate the case in which the local field corrections parameter is large enough to provide intrinsic optical bistability ($L > L_{th}$). In this situation, one expects to find again the typical decrease of the field amplitude with the Doppler width for the stable lasing solution, as in Figure 4.3. In addition, for a suitable set of parameters and in the limit of small Doppler widths, the non-lasing solution for the amplitude of the field has to be found according to the results shown in Chapter 3, in which bistability of the laser is found for certain values of the cavity detuning parameter $\tilde{\Delta}_c$.

In Figure 4.6 the numerical solution for the modulus of the amplitude of the generated field α is plotted (black circles) as a function of the Doppler width $\tilde{\Delta}\omega_d$ for $b = 0.5$, $r = 0.1$, $\tilde{\sigma} = 0.5$, $p = 250$, $\tilde{\Delta}_c = -1.5$ and different values of the local field corrections parameter, (a) $L = 150$, (b) $L = 165$, (c) $L = 200$, for which the system exhibits intrinsic optical bistability. The case without local field corrections is also shown with a dashed line. In all cases, for small Doppler widths, we observe the presence of both the lasing (upper) and the non-lasing (lower) solutions, and reaching one or the other depends only on the initial conditions. For the upper solutions, a decrease of the amplitude of the field with increasing the Doppler width is observed. In addition, note that in all figures, there is a certain threshold value of the Doppler width $\tilde{\Delta}\omega_d^{th}$ above which the bistability disappears (vertical dotted lines). Focusing on the Figure 4.6(a), we observe that the decrease of the lasing solution with the Doppler width shows a similar profile to the cases of $L < L_{th}$ analysed in the last subsection (Figure 4.3). In the same figure, the lower solution is found only below the threshold value of the Doppler width ($\tilde{\Delta}\omega_d^{th} \simeq 3$) above which the bistability disappears. In Figure 4.6(b), the threshold width, above which there is no bistability, is larger than in the case of $L = 150$ ($\tilde{\Delta}\omega_d^{th} \simeq 3.5$), and we observe that the higher lasing solution disappears above this threshold value, while the lower solution in this case is found above the

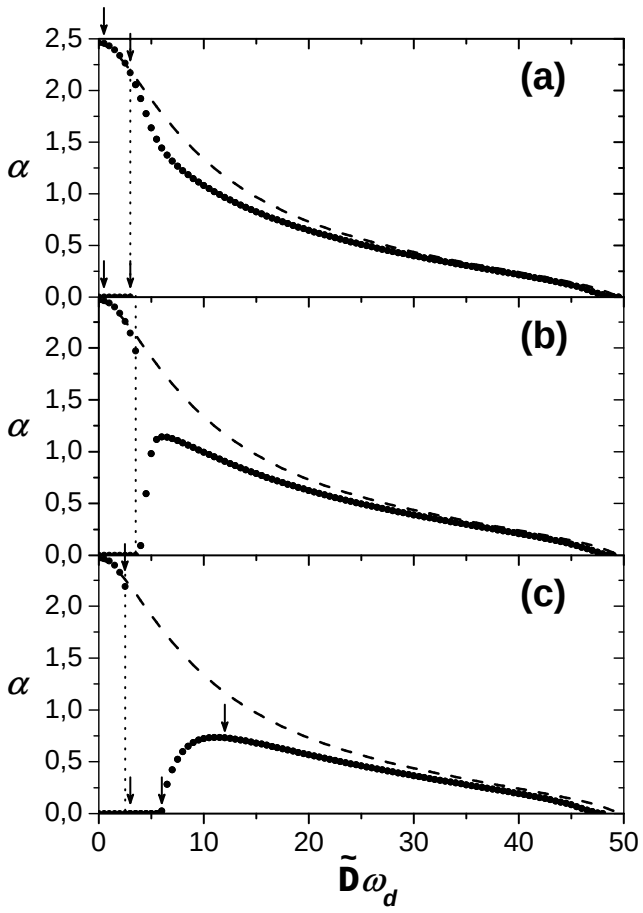

Figure 4.6: Modulus of the amplitude of the generated field as a function of the Doppler width for $b = 0.5$, $r = 0.1$, $\tilde{\sigma} = 0.5$, $p = 250$, $\tilde{\Delta}_c = -1.5$, and (a) $L = 150$, (b) $L = 165$, (c) $L = 200$. The case of $L = 0$ is also shown with dashed lines. The arrows drawn in the cases (a) and (c) indicate the Doppler widths corresponding to Figures 4.7-4.8.

threshold, and in a certain Doppler width range it even takes increasing values of the field amplitude with the Doppler broadening. However, for larger values of the Doppler width, the amplitude of the field decreases following a similar behaviour to Figure 4.3. Figure 4.6(c) is similar to the previous one, but here the threshold value of the Doppler width is smaller than in the previous cases ($\tilde{\Delta}\omega_d \simeq 2.5$). Moreover, the Doppler width value at which the amplitude of the lower solution begins to increase is larger than in the case of $L = 165$. Therefore, there is a certain range of Doppler widths at which the laser does not emit, and by increasing the Doppler width parameter the laser can be turned on.

The behaviour of the amplitude of the field with the Doppler width shown in Figure 4.6 can be interpreted by studying the behaviour of the population inversion $d(v)$ and the gain $g(v)$ for the different velocity classes, considering the upper and the lower solutions at the steady-state. In Figure 4.7 we plot $d(v)$ and $g(v)$, as a function of the Doppler shift Ωv, for $L = 150$ and different values of the Doppler width: (a) $\tilde{\Delta}\omega_d = 0.5$ (upper solution), (b) $\tilde{\Delta}\omega_d = 3$ (upper solution), (c) $\tilde{\Delta}\omega_d = 0.5$ (lower solution), (d) $\tilde{\Delta}\omega_d = 3$ (lower solution) and the rest of parameters as in Figure 4.6. In Figure 4.8 we show the population inversion $d(v)$ and the gain $g(v)$ as a function of the Doppler shift for $L = 200$ and (a) $\tilde{\Delta}\omega_d = 2.5$ (lasing solution), (b) $\tilde{\Delta}\omega_d = 3$, (c) $\tilde{\Delta}\omega_d = 6$, (d) $\tilde{\Delta}\omega_d = 12$ and the rest of parameters as in Figure 4.6(c). All the cases in Figures 4.7 and 4.8 are marked with arrows in Figures 4.6(a) and (c). The horizontal and the vertical dashed lines correspond to the value of the laser losses per velocity class, and to the position of the resonance velocity Ωv_{res}, respectively.

Considering the upper solution at $L = 150$ we find, for small Doppler widths (Figure 4.7(a)), that the spectral hole burning does not appear in the population distribution, and that the maximum of the gain distribution does not correspond with the resonance velocity (vertical dashed line). This is due to the fact that, for small Doppler widths, the minimum of the hole position is significantly shifted from the resonance velocity due to the distribution of atomic velocities, as we have commented in the discussion of Figure 4.1. By increasing the Doppler width (Figure 4.7(b)) we observe that, as expected, the total gain diminishes whereas the total population inversion increases. A displacement of the resonance velocity towards negative values of the Doppler shift, due to the increase of the Lorentz shift, is also observed. On the contrary, for the case of the lower solution we observe that, in the limit of small Doppler widths, the resonance velocity is far away from the central velocity (Figure 4.7(c)) because, since the laser is not emitting, the total population inversion equals the pump rate, and hence the Lorentz shift is maximum. In this situation practically there are no atoms that fulfill the resonance condition and hence that contribute to the total gain. However, when increasing the Doppler width, the distribution of velocities is broadened and at a certain value of $\tilde{\Delta}\omega_d$ there are enough atoms contributing to the total gain to compensate the losses (Figure 4.7(d)). When this occurs the amplitude of the field begins to increase. The growth of the field amplitude is so abrupt due to the fact that, for the value of the local field corrections considered ($L = 150$), the Doppler width at which the laser begins to turn on is small, and this implies that

the number of atoms per velocity class increase abruptly as the resonance velocity approaches to the central velocity, leading to a rapid growth of the total gain.

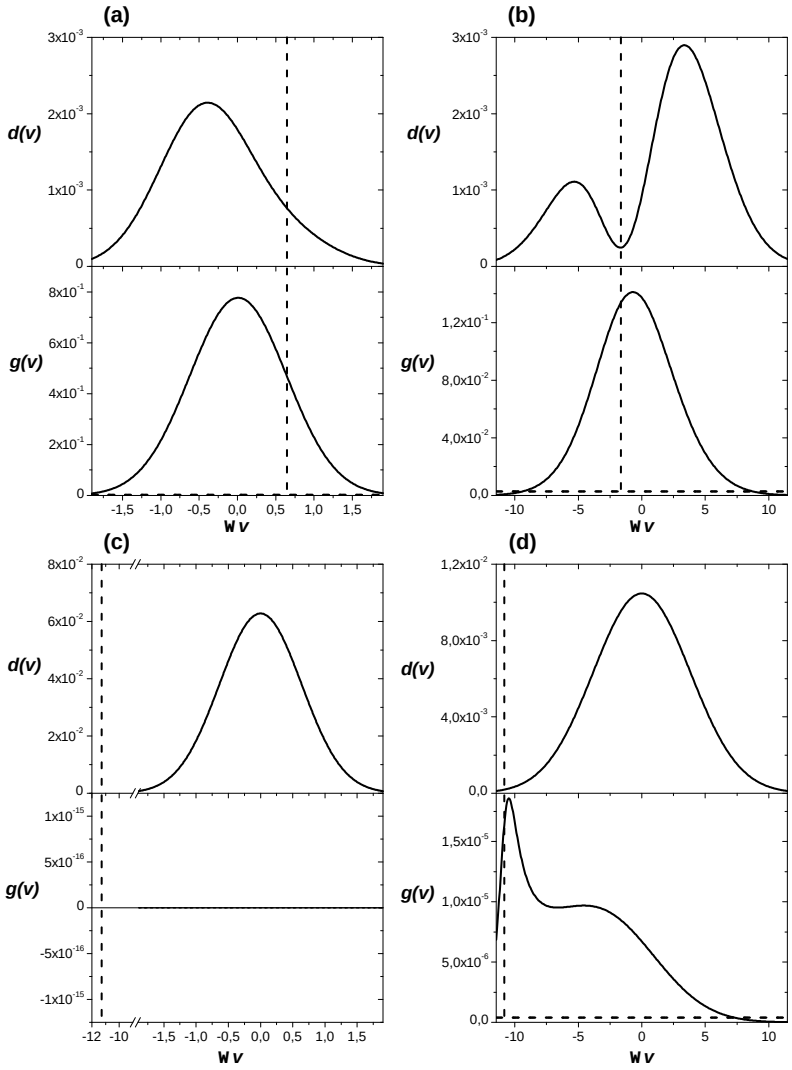

Figure 4.7: Population distribution and gain coefficient as a function of the Doppler shift for (a) $\tilde{\Delta}\omega_d = 0.5$ (upper solution), (b) $\tilde{\Delta}\omega_d = 3$ (upper solution), (c) $\tilde{\Delta}\omega_d = 0.5$ (lower solution), (d) $\tilde{\Delta}\omega_d = 3$ (lower solution) and the rest of parameters as in Figure 4.6(a).

In the cases shown in Figures 4.6(b)-(c), corresponding to local field corrections values of $L = 165$ and $L = 200$, respectively, we have observed that contrarily to the case presented in Figure 4.6(a), here is the upper solution which disappears above the threshold Doppler width. This can also be interpreted, as in the previous

case, in terms of the population distribution $d(v)$ and the gain $g(v)$ per velocity class. Although the total population inversion d_T is small, for high values of L, the Lorentz shift can be large enough to cause that only a small number of atoms contribute to the total gain. This produces a reduction of the amplitude of the field, which at the same time leads to an increase of the total population inversion, and hence the Lorentz shift increases even more. This situation leads to a rapid decrease of the amplitude of the field with the Doppler width, and eventually can lead to the switching off of the laser as shown in Figure 4.6(c). This effect is shown in Figures 4.8(a)-(b), where $d(v)$ and $g(v)$ are plotted for $L = 200$ and Doppler widths $\tilde{\Delta}\omega_d = 2.5$ and $\tilde{\Delta}\omega_d = 3$, respectively. Whereas in the former the position of the resonance velocity (vertical dashed line) is relatively close to the central velocity, in the latter, in which the Doppler shift has changed slightly, the vertical dashed line is far away from the wings of the velocity distribution. In addition, note that the values of $d(v)$ and $g(v)$ exhibited in both cases are consistent with the results for the amplitude of the field shown in Figure 4.6(c): for the case of $\tilde{\Delta}\omega_d = 2.5$, the maximum of the population distribution is smaller than in the case of $\tilde{\Delta}\omega_d = 3$, whereas the gain is larger in the first situation than in the latter. Contrarily, focusing on the lower solutions, the large L parameter favors the Doppler width at which the amplitude of the field grows, i.e., the Doppler width above which the total gain exceed the losses, being larger that in the previous case ($L = 150$), and consequently, the variation of the number of atoms per velocity class is smoother. This produces that the number of atoms that contribute to the total gain increases slowly with the Doppler width, as the resonance velocity move towards the central velocity and thus the increase of the lower solution is more gradual. In Figures 4.8(c)-(d) we have plotted $d(v)$ and $g(v)$ for $L = 200$ and Doppler widths $\tilde{\Delta}\omega_d = 6$ and $\tilde{\Delta}\omega_d = 12$, respectively. We observe that the position of the resonance velocity in the first case is only slightly smaller that in the second one, due to the fact that the values of the total population inversion in both cases are very similar. However, in spite of the position of the resonance velocity is similar in both cases, the total gain is quite different because in the case of $\tilde{\Delta}\omega_d = 12$ there are more atoms satisfying the resonance condition than in the case with $\tilde{\Delta}\omega_d = 6$. After the growth of the lower solution, the field amplitude begins to decrease because the number of atoms per velocity class decrease with the Doppler width, and therefore the total gain is also diminished. In this situation, as we have seen in Figure 4.5, the position of the hole burned into the population distribution tends to a constant value, due to the fact that the total population

inversion equals the pump rate, and its depth approaches to zero because of the field attenuation, as the Doppler width increases.

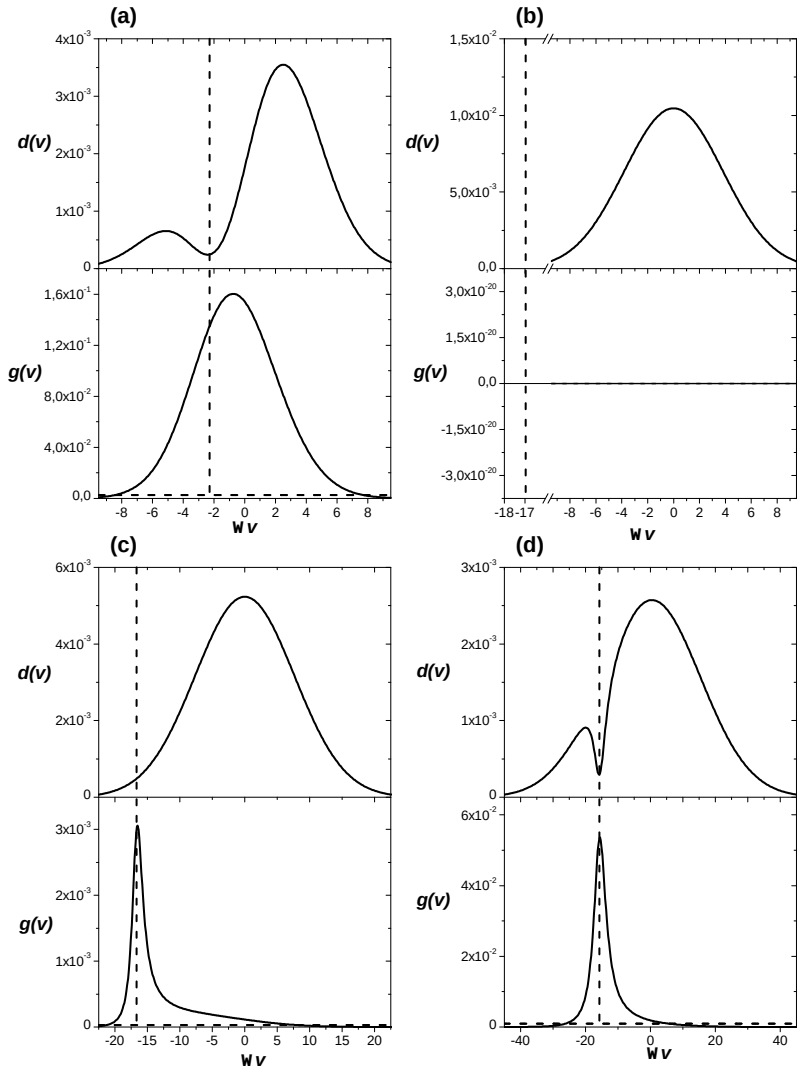

Figure 4.8: Population distribution and gain coefficient as a function of the Doppler shift for (a) $\tilde{\Delta}\omega_d = 2.5$ (lasing solution), (b) $\tilde{\Delta}\omega_d = 3$, (c) $\tilde{\Delta}\omega_d = 6$, (d) $\tilde{\Delta}\omega_d = 12$ and the rest of parameters as in Figure 4.6(c).

4.4 Realistic conditions

It has been shown in Chapter 3 that for a two-level laser, intrinsic optical bistability can be achieved by increasing the local field corrections parameter L, which

is proportional to the atomic density of the medium N and inversely proportional to the laser frequency ω_n, above a threshold value L_{th}. For a realistic set of parameters, e.g., the spontaneous emission γ and the pump Λ rates ~ 1 MHz, the coherence decay rate $\gamma_\perp \sim 1$ GHz, the reference density $N_0 \sim 10^{20}$ at/m^3, and the cavity losses $\sigma \sim 0.1$ $(\Omega\text{m})^{-1}$, this situation can be achieved by considering an infrared transition, $\omega_{ab} \sim 10^{11}$ Hz, and atomic densities of the order of $N \sim 10^{23}$ at/m^3. In this chapter it has been reported that the inclusion of Doppler broadening in the dense two-level laser leads to the disappearance of the intrinsic optical bistability, and eventually of the laser field, with increasing Doppler width. Taking parameters for the D_2 line of rubidium 87 [51], the bistability disappears for Doppler widths corresponding to temperatures of $\sim$ 1 K (see Figure 4.6). Although these values of the temperature are small, the corresponding Doppler widths are larger than the width due to the homogeneous broadening.[1] However, for the rubidium atom, the Doppler shift takes non-negligible values only for optical (or higher) frequencies, and consequently, the density has to be increased 3-4 orders of magnitude,[2] with respect the infrared case, to observe intrinsic optical bistability, which is clearly unrealistic. Therefore, we should consider alternative systems in which the density required to obtain intrinsic bistability could be reduced. In the last decade, some theoretical works [15–18] have explored the possibility of local field effects enhancement without necessarily increasing the density of the medium. While in the first two studies [15, 16], the resonant atoms were considered embedded in a dielectric host medium, in [17] the dense medium was considered to be formed by two different atomic species. Later, Afanas'ev *et al.* [18] showed that a dense ensemble of atoms modeled by multilevel quantum systems allows to reduce the condition reported in [8] for the appearance of intrinsic optical bistability. These possibilities should be considered when leading for more realistic systems in which our predictions apply.

[1] The temperature at which the Doppler width is comparable with the homogeneous width, for the D_2 line of rubidium 87 parameters [51], is $\sim 10^{-2}$ K.

[2] Note that $L \propto N/\omega_n$, with N the density of the medium and ω_n the frequency of the field.

5

Summary and Conclusions

In this research work we have considered a two-level gas laser within the Semiclassical framework, in the presence of local field corrections and Doppler broadening. In the following the main conclusions of each chapter will be summarized.

In Chapter 2 the physical system under investigation, consisting of a two-level active gas placed in a unidirectional ring laser cavity, has been discussed, and the model equations, i.e., the optical Bloch equations, describing the temporal dynamics of the system, have been derived. To obtain the equation for the time evolution of the field from the Maxwell equations, a single cavity longitudinal mode of an electromagnetic field has been considered under the Slowly Varying Envelope Approximation. The time evolution equations of the medium, i.e., the populations and the coherence equations, have been obtained using the Schrödinger-von Neumann-Liouville equation and assuming the Electric Dipole and Rotating Wave Approximations. The derivation of the optical Bloch equations has been performed in a self-consistent way, by assuming the polarization of the atomic medium as a source term in the Maxwell equations. Finally the Lorentz-Lorenz relation has been used in order to include the role of the local field corrections, accounting for near dipole-dipole interactions typically present in dense media. This correction, which appears in the equations through the local field corrections parameter L, gives rise to a non-linear term in the atomic coherence time evolution equation that is interpreted as a non-linear detuning proportional to the population inversion d, known as the Lorentz shift ($\Delta^s = Ld$), and it is responsible for intrinsic optical bistability.

In Chapter 3 the steady-state solutions of the model equations derived in Chapter 2 have been found. Both the number of stationary solutions and the resonance profile of the atomic transition have been studied as a function of the local field corrections (L) and the cavity detuning ($\tilde{\Delta}_c$) parameters, for three different cases:

(i) the two-level medium interacting with a weak probe electromagnetic field, (ii) the medium in the presence of a external strong field, and (iii) the two-level medium generating a laser field. In the first situation, in which a weak probe field is externally applied to the two-level dense medium, only one real steady-state solution is found, and a linear displacement of the whole resonance curve, i.e., the imaginary part of the coherence as a function of the field detuning, is observed when L increases. This is the well known static Lorentz shift. However, if the applied field is strong enough (ii), the Lorentz shift varies with the population difference and then the displacement of the base of the resonance curve, where the population inversion is maximum, is larger than in the peak, where the population difference is minimum. This phenomenon is known as dynamic Lorentz shift. In this situation, for large enough values of the local field parameter, three different steady-state solutions of the optical Bloch equations can be found. This situation is quite similar to the lasing case (iii), in which the population inversion depends on the generated intensity, and thus the dynamic Lorentz shift is also observed. However, in the lasing case a trivial steady-state solution, corresponding to a non-lasing state, is always present. In addition, a non-trivial steady-state solution, which corresponds to a lasing state, is also found within a certain range of the cavity detuning parameter ($\tilde{\Delta}_{c0} \leqslant \tilde{\Delta}_c \leqslant \tilde{\Delta}_{c2}$). In this case, for small values of the local field corrections we observe, as in (ii), a displacement of the basis of the resonance profile, i.e., of the amplitude of the field versus the cavity detuning. However, when the local field parameter is increased above a threshold value L_{th}, this displacement is such that another lasing solution emerges for certain values of the cavity detuning ($\tilde{\Delta}_{c1} \leqslant \tilde{\Delta}_c < \tilde{\Delta}_{c2}$ with $\tilde{\Delta}_{c0} < \tilde{\Delta}_{c1}$). Thus, three different steady-state solutions coexist in a certain cavity detuning range: a trivial solution, a lasing solution with the higher intensity (HI lasing solution), and a lasing solution with the lower intensity (LI lasing solution). To study the stability of these solutions a linear stability analysis has been performed. The analysis has revealed that while the HI lasing solution is always stable, the LI lasing solution is unstable. Moreover, the trivial solution is also unstable in the cavity detuning range in which it coexists only with the HI lasing solution, i.e., for $\tilde{\Delta}_{c0} < \tilde{\Delta}_c < \tilde{\Delta}_{c1}$. In conclusion, for the cavity detunings in which the three solutions coexist, the trivial and the HI non-trivial solution are stable, while the LI non-trivial solution, is always unstable, i.e., we have obtained that the two-level laser exhibits bistability in the stationary regime when the local field corrections parameter is above a threshold value, $L > L_{th}$, for a certain range of cavity detunings.

In Chapter 4 the role of the Doppler effect in the dynamics of a dense two-level laser has been studied. First, the Doppler broadening has been introduced by considering the two-level atomic gas placed in a vapor cell at finite temperature and in thermal equilibrium. In this situation, the velocity distribution of the atoms in the propagation direction of the field is given by a Maxwell distribution. The atomic motion implies that, as a consequence of the Doppler effect, each atom sees the laser field with a different frequency. This frequency distribution as a function of the atomic velocities gives rise to a Gaussian broadening of the resonance line known as Doppler broadening. It has been shown that, when dealing with an intense laser field, this kind of inhomogeneous broadening gives rise to the phenomenon of hole burning. This phenomenon consists in the saturation of the transition of only a certain velocity class of atoms by a strong laser field. The atoms whose transition is saturated are those with a velocity such that the laser is resonant with them. This preferential saturation produces a hole burned in the population distribution, centered at the resonance velocity, whose depth depends on the intensity of the generated field. Accordingly, we have modified the optical Bloch equations with local field corrections, in order to take into account the Doppler effect. It has been shown that the inclusion of this effect gives rise to a velocity dependent field detuning, and consequently the population inversion and the coherence become also velocity dependent. This velocity dependent detuning along with the Lorentz shift due to the local field corrections can be interpreted as an effective detuning that modifies the position of the hole burning. The numerical results, obtained by the integration of the evolution equations of the considered dense two-level laser in the presence of the Doppler broadening, show this dependence, as well as a linear displacement of the hole burning position with the parameter L with $L < L_{th}$, for a fixed value of the Doppler width. This linear displacement is due to the fact that for small values of the effective detuning, the hole is centered near the central velocity and therefore the amplitude of the field, and hence the total population inversion, are almost constants. For this reason, the Lorentz shift only varies with L. It has been also shown that another cause for the hole displacement is the variation of the Doppler width. Since the amplitude of the field decreases with the Doppler width, the total population inversion, as well as the Lorentz shift, varies leading to a displacement and to a depth reduction of the hole.

Next, the density of the gaseous medium has been assumed to be high enough to produce intrinsic optical bistability and the evolution of the absolute value of

the field amplitude with the Doppler width has been analysed. Specifically, three different cases with $L > L_{th}$ have been considered: (a) $L = 150$, (b) $L = 165$, and (c) $L = 200$. In all cases, in the limit of small Doppler widths, both the lasing and the non-lasing stable solutions found in Chapter 3, appear for different initial conditions. In the lasing case, a decrease of the field amplitude with increasing the Doppler width is observed. Nevertheless, a sudden disappearance of the intrinsic optical bistability has been observed above a certain value of the Doppler width. Whereas for the case (a) the loss of the intrinsic bistability is produced by means of the disappearance of the lower solution, while the lasing solution decreases its amplitude with increasing Doppler widths, in cases (b) and (c) is the higher solution that is not found above a certain value of the Doppler width. In the last two cases we have seen that, within a range of Doppler widths the lower solution increases, whereas for values above this region it decreases following a similar profile to the cases with $L < L_{th}$. The behaviour exhibited by the steady-state solutions of the field amplitude as a function of the Doppler width has been interpreted in terms of the population inversion and gain distributions as a function of the atomic velocity. We have seen that, considering the lower solution in the case of $L = 150$ and for small Doppler widths, the position of the resonance velocity is far away from the central velocity because of the large Lorentz shift. Therefore, the number of atoms that satisfies the resonance condition, i.e., that contributes to the total gain, is not sufficient to compensate the laser losses, and in this situation the laser does not emit. However, increasing the Doppler width up to a certain value, the broadening of the velocity distribution is such that there are enough atoms contributing to the total gain to exceed the losses, and hence the amplitude of the field begins to increase. For the values of L considered in this case, the Doppler width at which the solution begins to increase is so small that the variation of the number of atoms per velocity class is important, and therefore the total gain, and hence the amplitude of the field, increases rapidly with the Doppler width. For the same reason, the upper solution in the cases with $L = 165$ and $L = 200$ decreases abruptly. The gradual increase of the lower solution in the last two cases is due to the fact that for large L parameters, the Doppler width at which the solution begins to grow is so large that the variation of the number of atoms per velocity class is small. Therefore the number of atoms that satisfies the resonance condition increases progressively. Nevertheless, when the Doppler width reaches a certain value, the number of atoms at the resonance velocity class begins to decrease, and then the amplitude of the field diminishes

with the Doppler width.

Finally, a brief discussion on the possibility to observe the studied effects in realistic systems is performed. We obtain that intrinsic optical bistability might appear in a two-level laser in the infrared domain ($\omega_{ab} \sim 10^{11}$ Hz) for atomic densities of the order $N \sim 10^{23}$ at/m^3, for which the local field corrections are above the predicted threshold. When the Doppler broadening is taken into account, we find that the temperatures for which the system exhibits intrinsic optical bistability are of the order of ~ 1 K. Note that although these temperatures are very low, they provide Doppler widths larger than the natural width. Unfortunately, for Doppler broadenings corresponding to optical transitions, the requirements for the density to obtain intrinsic optical bistability are clearly unrealistic. Although these results indicate that the observation of the intrinsic bistability in a Doppler broadened two-level laser is not feasible, we plan to explore the possibility of using alternative systems as, for instance, the theoretical models of Crenshaw and Bowden [15], Crenshaw, Bowden and Sullivan [17] and Afanas'ev *et al.* [18] where the effects of the local field corrections are enhanced without increasing the density of the medium by means of considering the resonant atoms embedded in a dielectric host medium, multicomponent media systems, or atomic coherence effects in multilevel quantum systems, respectively. Note, however, that the other effect predicted in the dense two-level laser in the presence of Doppler broadening, the displacement of the hole burning is a thresholdless phenomenon. Therefore, it should be possible to observe it for much lower densities that the intrinsic optical bistability.

Bibliography

[1] M. O. Scully and M. S. Zubairy, *Quantum Optics* (Cambridge University Press, New York, 1997).

[2] P. Meystre and M. Sargent-III, *Elements of Quantum Optics* (Springer-Verlag, 1990).

[3] M. Sargent-III, M. O. Scully, and J. W. E. Lamb, *Laser Physics* (Addison-Wesley, 1993).

[4] J. D. Jackson, *Classical Electrodynamics (2nd Edition, Chap. 4)* (Weley, 1975).

[5] I. V. Jyotsna and G. S. Agarwal, Phys. Rev. A **53**, 1690 (1996).

[6] R. Friedberg, S. R. Hartmann, and J. T. Manassah, Phys. Rep. **C7**, 101 (1973).

[7] C. M. Bowden and J. P. Dowling, Phys. Rev. A **47**, 1247 (1993).

[8] R. Friedberg, S. Hartmann, and J. T. Manassah, Phys. Rev. A **40**, 2446 (1989).

[9] R. Friedberg, S. Hartmann, and J. T. Manassah, Phys. Rev. A **42**, 494 (1990).

[10] C. M. Bowden, A. Postan, and R. Inguva, J. Opt. Soc. Am. B **8**, 1081 (1991).

[11] M. E. Crenshaw, M. Scalora, and C. M. Bowden, Phys. Rev. Lett. **68**, 911 (1992).

[12] R. Inguva and C. M. Bowden, Phys. Rev. A **41**, 1670 (1990).

[13] C. M. Bowden and C. C. Sung, Phys. Rev. A **19**, 2392 (1979).

[14] F. A. Hopf, C. M. Bowden, and W. H. Louisell, Phys. Rev. A **29**, 2591 (1984).

[15] M. E. Crenshaw and C. M. Bowden, Phys. Rev. A **53**, 1139 (1996).

[16] J. T. Manassah, Opt. Commun. **191**, 435 (2001).

[17] M. E. Crenshaw, K. U. Sullivan, and C. M. Bowden, Opt. Express **1**, 152 (1997).

[18] A. A. Afanas'ev, A. G. Cherstvy, R. A. Vlasov, and V. M. Volkov, Phys. Rev. A **60**, 1523 (1999).

[19] F. A. Hopf and C. M. Bowden, Phys. Rev. A **32**, 268 (1985).

[20] Y. Ben-Aryeh, C. M. Bowden, and J. C. Englund, Phys. Rev. A **34**, 3917 (1986).

[21] M. E. Crenshaw and C. M. Bowden, Opt. Commun.. 63 **179**, 63 (2000).

[22] A. S. Manka, J. P. Dowling, C. M. Bowden, and M. Fleischhauer, Phys. Rev. Lett. **73**, 1789 (1994).

[23] J. T. Manassah and I. Gladkova, Opt. Commun. **185**, 125 (2000).

[24] J. Kästel and M. Fleischhauer, Phys. Rev. A **76**, 062509 (2007).

[25] J. J. Maki, M. S. Malcuit, J. E. Sipe, and R. W. Boyd, Phys. Rev. Lett. **67**, 972 (1991).

[26] M. P. Hehlen, H. U. Gudel, Q. Shu, J. Rai, S. Rai, and S. C. Rand, Phys. Rev. Lett. **73**, 1103 (1994).

[27] V. A. Sautenkov, H. van Kampen, E. R. Eliel, and J. P. Woerdman, Phys. Rev. Lett. **77**, 3327 (1996).

[28] J. Rai and C. M. Bowden, Phys. Rev. A **46**, 1522 (1992).

[29] J. P. Dowling and C. M. Bowden, Phys. Rev. Lett. **70**, 1421 (1993).

[30] F. Sanchez, M. Brunel, and G. Martel, Phys. Rev. A **61**, 033817 (2000).

[31] M. Fromager, M. Brunel, and F. Sanchez, Phys. Rev. A **61**, 053804 (2000).

[32] O. G. Calderón, E. Cabrera, M. Antón, and J. M. Guerra, Phys. Rev. A **67**, 043812 (2003).

[33] V. Ahufinger, J. García-Ojalvo, J. Mompart, M. C. Torrent, R. Corbalán, and R. Vilaseca, Phys. Rev. Lett. **91**, 083901 (2003).

[34] C. M. Bowden, S. Singh, and G. P. Agarwal, J. Mod. Opt. **42**, 101 (1995).

[35] J. Guo, A. Gallagher, and J. Cooper, Opt. Commun. **131**, 219 (1996).

[36] J. W. R. Bennett, Phys. Rev. **126**, 580 (1962).

[37] V. Letokhov and V. Chebotayev, *Nonlinear Laser Spectroscopy* (Springer-Verlag, 1977).

[38] T. W. Hänsch, M. H. Nayfeh, S. A. Lee, S. M. Curry, and I. S. Shahin, Phys. Rev. Lett. **32**, 1336 (1974).

[39] R. M. Macfarlane and R. M. Shelby, Phys. Rev. Lett. **42**, 788 (1979).

[40] J. Lamb, Phys. Rev. **134**, A1429 (1964).

[41] T. W. Hänsch, I. S. Shahin, and A. L. Schawlow, Phys. Rev. Lett. **27**, 707 (1971).

[42] M. S. Sorem and A. L. Schawlow, Opt. Commun. **5**, 148 (1972).

[43] A. A. Gorokhovski, R. K. Kaarli, and L. A. Rebane, JETP Lett. **20**, 216 (1974).

[44] K. Naoe, L. G. Zimin, and Y. Masumoto, Phys. Rev. B **50**, 18200 (1994).

[45] M. O. Scully and M. S. Zubairy, *Persistent spectral hole burning; science and application (W. E, Moerner Ed.)* (Springer, Berlin, 1988).

[46] T. Kawazoe and Y. Masumoto, Phys. Rev. Lett. **77**, 4942 (1996).

[47] B. S. Ham, M. S. Shahriar, and P. R. Hemmer, Opt. Lett. **22**, 1138 (1997).

[48] R. N. Shakhmuratov, A. Rebane, P. Mégret, and J. Odeurs, Phys. Rev. A **71**, 053811 (2005).

[49] G. S. Agarwal and T. N. Dey, Phys. Rev. A **68**, 063816 (2003).

[50] R. M. Camacho, M. V. Pack, and J. C. Howell, Phys. Rev. A **74**, 033801 (2006).

[51] D. A. Steck, Available online at http://steck.us/alkalidata (revision 2.0.1, 2 May 2008) (2008).